A Mathematical Model for Chemo-Immunotherapy of Cancer Considering Macrophages Polarization and Cytokine Dynamics

Negin Darandis[1], Mostafa Nazari[1*]
[1]Faculty of Mechanical Engineering, Shahrood University of Technology, Shahrood, Iran, POB 3619995161
[1*]Corresponding author: nazari_mostafa@shahroodut.ac.ir

Abstract:
Currently, immunotherapy represents a cancer treatment and is commonly considered in combination with chemotherapy. This approach is particularly relevant for malignancies associated with impaired immune function. In this work, an ordinary differential equation (ODE) model is formulated as a mathematical framework for describing interactions between tumor and immune cells. Macrophage polarization together with cytokine dynamics is incorporated through pharmacokinetic-pharmacodynamic assumptions to provide a more detailed representation of tumor-immune interactions. The limited number of studies addressing these mechanisms within chemo-immunotherapy models motivated the development of this ODE framework. The positivity of solutions, equilibrium states, and their stability properties are analyzed. Furthermore, sensitivity of the final tumor population and the response time to initial conditions and parameter values is examined. The initial state of the adaptive immune system, as well as parameters governing tumor-cell proliferation, tumor carrying capacity, and the fractional exponent for CD8+ T-cell-mediated tumor-cell killing, strongly influences both the final tumor burden and the tumor-growth response time. Subsequently, numerical simulations are conducted for pulsed chemotherapy, pulsed immunotherapy, and combined chemo-immunotherapy, and the resulting responses are compared. Three patients exhibiting different immune responses are considered to demonstrate how immune activity can affect treatment strategies. Numerical results indicate that combining immunotherapy with chemotherapy can enhance tumor-control dynamics. Furthermore, the simulations reveal that immune-system strength plays a substantial role in determining cancer treatment outcomes.

Keywords: Mathematical model, Chemo-immunotherapy, cancer, tumor-immune interaction

1. Introduction

Cancer is the second cause of death in the world [1]. Cancer cells can grow rapidly at their site and can metastasize to other organs through blood circulation or the lymphatic system [2]. When a cell mutates, it may become cancerous. The immune system tries to diminish this type of cells by infiltrating them and producing proteins which eradicate the membrane of the cancer cell, and releasing enzymes for cancer cell apoptosis [3].

The dynamics of the tumor-immune interaction are very complex, and knowing these dynamics helps us to better model. The body defense system has two parts: innate and adaptive. The general defense is applied quickly by the innate immune system. Macrophages, neutrophil leukocytes, and natural killer (NK) cells belong to the innate immune system. The response of the adaptive immune system takes longer. The adaptive immune system response remains a memory for the future. Dendritic cells (DCs) and B lymphocytes belong to the adaptive immune system. Antibody production for a specialized pathogen is the duty of B lymphocytes, while naïve T lymphocytes differentiate into specialized subsets, including cytotoxic T lymphocytes (CD8+ T cells), helper T cells (CD4+ T cells), regulatory T cells (Tregs), and memory T cells [4, 5]. Dendritic cells initiate adaptive response and activate naïve T cells [4]. Any cell not known as belonging to the host organism is removed by CD8+ T cells (Cytotoxic T lymphocytes) by expressing a unique antigen-binding molecule.

The two cells which have significant roles in the establishment of the immune response are type-1 helper T cells (Th1 cells) and regulatory T cells (Regulatory T cells (Regulatory T cells (Tregs))). T helper (Th) cells and T regulatory cells (Regulatory T cells (Tregs)) are categorized into CD4+ T cells. Th cells are adjusted by Regulatory T cells (Regulatory T cells (Tregs)). The adaptive immune system is controlled against pathogens by Th cells.

ACCEPTED MANUSCRIPT

Macrophages are activated by Th cells to annihilate ingested microbes. Moreover, B cells and cytotoxic T lymphocytes (CTLs) are activated to secrete antibodies and eliminate infected target cells, respectively.

Antigen-specific effector cells activate the immune response by the help of Th1 cells. Suppression lymphocytes such as Regulatory T cells (Tregs) preserve self-tolerance by applying a regnant negative regulation on other immune cells, such as CTLs [6, 7].

Cytokines, which are secreted by different molecules for the regulation of the immune system, have a significant effect on the performance of the immune system [8][15]. They can be categorized into different classes such as interleukins (IL), transforming growth factors (TGFs), tumor necrosis factors, colony-stimulating factors, and interferons (IFNs) [9].

The complex dynamics of cancer depends on many cytokine-driven factors that may reinforce or weaken the immune system by anti-tumor or pro-tumor phenotypes. The improvement of the natural killer activities by activation of CD8+ T cells is done by secretion of interleukin-12 (IL12) [8]. Interleukin-10 (IL10) is produced in the presence of IL12 and has side effects on the performance of IL12 [8, 10]. Interleukin-2 (IL-2), primarily produced by activated $CD4^+$ T helper cells, is a key cytokine involved in the activation, proliferation, survival, and differentiation of $CD8^+$ cytotoxic T lymphocytes (CTLs) [11].

The phagocytizing of cancer cells may be done directly by other immune cells such as macrophages. Macrophages can exert antitumor activity either by direct cell-to-cell cytotoxic interactions or by releasing soluble effector molecules, including nitric oxide, reactive oxygen species, and various pro-inflammatory cytokines.

However, M2 macrophages have pro-tumor activity by releasing angiogenic and immunosuppressive agents. It has been shown that increasing the M1-to-M2 macrophage ratio enhances anti-tumor immune responses and increases the probability of tumor elimination by the immune system, whereas a low M1/M2 ratio is generally associated with tumor progression and immune suppression [6, 10]. Lampropoulos et al. [12] developed a spatio-temporal tumor growth model incorporating M1 and M2 macrophages, showing that macrophage polarization and spatial heterogeneity strongly influence tumor progression and micro environmental dynamics. Recent advances in cancer immunology have demonstrated that macrophages are among the most influential components of the tumor microenvironment. Through their ability to switch between anti-tumor (M1) and pro-tumor (M2) phenotypes, macrophages regulate immune activation, cytokine production, and therapeutic outcomes. These findings motivate the inclusion of macrophage polarization and immune-regulatory mechanisms in mathematical models of tumor–immune interactions and chemo-immunotherapy [13].

IL12 is secreted by M1 macrophage and causes the differentiation of naïve helper T cells into type-1 T helper (Th1) cells. Moreover, IFN-Υ that is secreted by Th1 cells leads to M1 macrophage phenotype reinforcement. Such loops are called positive feedback loops and cause tumor elimination.

Moreover, the cytokines interleukin-4 (IL4) and interleukin-6 (IL6) are secreted by M2 macrophages [14] [15]. They cause the differentiation of immature helper T cells into type-2 T helper (Th2) cells. Naïve helper T cells are converted to Regulatory T cells (Tregs), and B cells to Bregs by TGF-β, which is secreted by M2 macrophages and Th2 cells [16]. Also, interleukin-10 (IL10) and TGF-β secreted by Regulatory T cells (Tregs) and Bregs, reinforce the Th2 phenotype. Moreover, Th2 cells reinforce the M2 phenotype and finally cause pro-tumor activity. Regulatory T cells (Tregs) and Bregs reinforce each pro-tumor activity in the presence of IL-10 and TGF-β [17, 18]. TGF-β and IL6 cause M2 polarization and create an immune-suppressive environment. The production of a T cell-stimulating cytokine such as IL12 is one of the most important features of M1 macrophages. However, the activities of IL12 are down-regulated by M2 macrophages which are linked to the profuse production of IL10. More information and thorough review of these interactions is provided in [19]. Zhang and Li [20] demonstrated that the interactions between tumor cells and immune populations play a decisive role in determining cancer progression and therapeutic outcomes. Their results highlighted the importance of immune regulation in shaping tumor dynamics. Consistent with these observations, our results indicate that immune-related mechanisms, including immune strength, cytokine-mediated signaling, and macrophage polarization, significantly influence tumor evolution. In particular, the balance between M1 and M2 macrophages was found to be a critical factor governing the transition between anti-tumor and pro-tumor immune responses.

ACCEPTED MANUSCRIPT

Surgery has a remarkable scar and needs more surgery to decrease recurrence risk. Moreover, it is useful for removing the tumor cells from the vicinity of the organ. Radiotherapy is also used for removing tumor cells from the organ locally and used after surgery [21]. Injection of drugs is used in chemotherapy to kill or slow the rapid growth of tumor cells. However, Chemo-drugs kill both healthy and tumor cells [22][23]. Immunotherapy is used along with chemotherapy to reduce its side effects [24]. Immunotherapy reinforces the activity of immune cells. Unlike radiotherapy, oncologic chemotherapy and immunotherapy knowledge is not clearly obvious due to the drug-related biochemistry included for allowing accurate quantification of dose-response. This problem in mixed chemo-immunotherapy is more complicated. The questions about the amount of chemo-drug dose and its period remain mostly empirical over the years [25]. Cancer immunotherapy has emerged as a promising treatment strategy that harnesses the immune system to recognize and eliminate tumor cells [26]. Unlike conventional therapies that directly target cancer cells, immunotherapy seeks to enhance anti-tumor immune responses or alleviate immunosuppressive mechanisms within the tumor microenvironment. Several immunotherapeutic approaches, including immune checkpoint inhibitors, adoptive cell therapies, and cytokine-based treatments, exert their effects through modulation of immune-cell populations and cytokine networks.

Nevertheless, the ordinary differential equations (ODEs) mathematical models can be used to extract key features of cancer [27, 28]and to develop its general laws. These models can be used to develop treatment strategies based on optimization methods [29, 30]. Many mathematical models are presented to show the tumor-immune interaction. The interaction between tumor cells and effector cells (cytotoxic T lymphocytes) are simply modeled with Kuznetsov et al. [31]. Interleukin-2 produced by CD4+ cells are added by Kirschner and Panetta [32]. The previous approach is modified by Dong et al. [33]by regarding the population of CD4+ helper cells as a state, instead of the interleukin concentration. The effect of naïve T cells and effector cells to examine the chronic myelogenous are introduced by Moore and Li [34]. De Pillis et al. introduced a mathematical framework for tumor–immune interactions involving three principal populations: tumor cells, healthy cells, and immune cells [35, 36]. A more detailed representation of host immunity was later developed in [37], by incorporating both innate and adaptive components, specifically natural killer (NK) cells and CD8+ T lymphocytes. Innate immune cells are continuously present within the host, whereas other immune populations may become activated or recruited following the introduction of an external stimulus. In the formulation of [37], NK-cell generation is represented by a constant source term. In contrast, the model proposed in [38]introduces circulating lymphocytes as an additional state variable, allowing their contribution to the production of NK cells to be explicitly considered. Furthermore, immunotherapy-related effects are incorporated into the tumor–immune dynamics in [38, 39]. However, the effect of macrophages polarization and cytokine dynamics are not considered. These have a significant role in tumor-immune interaction which is considered in the present research.

Several studies on chemo-immunotherapy modeling are presented. Although chemo-immunotherapy becomes an essential need for cancer treatment [40], only few researches are aimed at modeling [25, 39, 41, 42]. One of the major points of our research is to contribute to covering these gaps by regarding more incorporated immune cells.

The present study differs fundamentally from our previous work [42] in its focus on combined chemo-immunotherapy, comprehensive equilibrium analysis including tumor-present states, and systematic evaluation of treatment responses under different initial conditions and immune strengths.

In the present study, a system of ordinary differential equations is formulated to characterize tumor–immune interactions by building upon the framework originally introduced by De Pillis and co-workers. The formulation is expanded to capture the phenotypic transition of macrophages and the regulatory effects of cytokine signaling. In addition, both tumor-suppressing and tumor-promoting functions of the relevant cellular populations are incorporated into the mathematical framework. The resulting interaction network, illustrated schematically in Fig. 1, provides the basis for constructing the governing equations of the proposed model.

As shown in Fig. 1, the tumor microenvironment was described by the interaction among the population of natural killer cells, CD8+ T cells, cytokines (such as IL2, IL10, etc.), macrophages, regulatory T cells, circulating lymphocytes, not including NK cells, Type-1 helper T-cell, and TGF- β.

ACCEPTED MANUSCRIPT

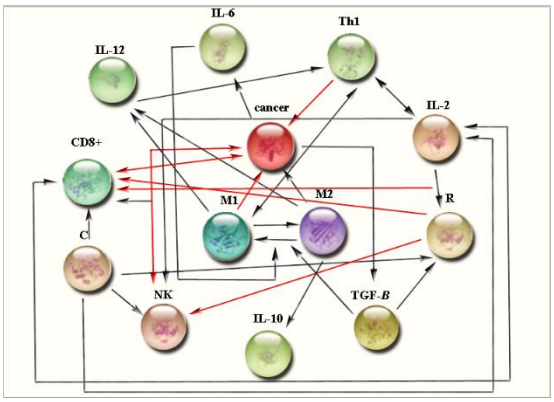


Fig. 1: The interaction of leading agents of the immune system with their interactions with the tumor cells. Red arrows are inhibitory effect and grey arrows are stimulatory effects.

We develop a model including significant agents of the immune system to study the dynamics of the tumor under chemo-immunotherapy more realistically. Afterward, the dynamics of the model is analyzed and the key parameters for cancer treatment are extracted. Then, based on the developed model, treatment strategies for patients with different immune system's ability are proposed as a novel insight. A detailed comparison of macrophage polarization models in cancer has been presented in Table 1.

Table 1: Detailed comparison of macrophage polarization models in cancer

Feature	Louzoun et al. (2014) [43]	den Breems & Eftimie (2016) [44]	Morales & Soto-Ortiz (2018) [19]	Lampropoulos et al. (2025) [12]	Bosque et al. (2025) [13]	Zhang et al. (2026) [20]	Present Study
Tumor cells	✓	✓	✓	✓	✓	✓	✓
M1 macrophages	✓	✓	✓	✓	✓	Limited/Indirect	✓
M2 macrophages	✓	✓	✓	✓	✓	Limited/Indirect	✓
Macrophage re-polarization (M1↔M2)	Partial	✓	✓	✓	✓	✗	✓
Tumor microenvironment regulation	Limited	Limited	Partial	Extensive	Extensive	Partial	Partial
Explicit cytokine dynamics	✗	Limited	✓ (IL-4, IL-10, TGF-β)	Partial	✓	Partial	✓
IL-12 dynamics	✗	✗	Limited	✗	Partial	✗	✓
IL-2 dynamics	✗	✗	✗	✗	✗	✗	✓
TGF-β dynamics	✗	✗	✓	Partial	✓	Partial	✓
Positive/negative immune feedback loops	✗	Partial	✓	Partial	Partial	Partial	✓
CTLs (CD8+ T cells)	Limited	✗	Limited	✗	Limited	✓	✓
Helper T cells (Th)	✗	✗	Limited	✗	Limited	✓	✓
Regulatory T cells (Regulatory T cells (Tregs))	✗	✗	Partial	✗	Limited	Partial	✓
Immune-strength formulation	✗	✗	✗	✗	✗	✗	✓
Chemotherapy	✗	✗	Treatment effect only	✗	✗	✗	✓
Immunotherapy	✗	✗	Partial	✗	Limited	Limited	✓

ACCEPTED MANUSCRIPT

Combined chemo-immunotherapy	✗	✗	✗	✗	✗	✗	✓
Reduced-order model using QSSA	✗	✗	✗	✗	✗	✗	✓
Local sensitivity analysis	✗	Limited	✗	Limited	Limited	Limited	✓
Global sensitivity analysis	✗	✗	✗	Limited	Limited	Limited	✓
Equilibrium and stability analysis	Limited	✓	Limited	✓	Limited	✓	✓
Treatment comparison under different immune conditions	✗	✗	✗	✗	✗	✗	✓
Treatment comparison under different tumor burdens	✗	✗	✗	✗	✗	✗	✓
Spatial model	✗	✗	✗	✓	✗	✗	✗
Main focus	Macrophage polarization	Repolarization and cancer outcomes	Cytokine-mediated macrophage dynamics	Spatial macrophage–tumor interactions	Macrophage-driven TME regulation	Tumor–immune interaction dynamics	Macrophage polarization, cytokine feedback, immune-strength dynamics, and chemo-immunotherapy

The proposed framework is a continuous-time, deterministic, non-spatial tumor–immune model formulated as a system of ordinary differential equations. The model describes population-level interactions among tumor cells, immune-cell populations, and cytokines, with emphasis on the temporal dynamics of the tumor microenvironment.

The proposed model is intended to represent generic tumor–immune interactions in solid tumors and is primarily designed to investigate the qualitative effects of immune-cell regulation, cytokine signaling, and macrophage polarization on tumor dynamics.

The main contributions of the proposed study compared with existing tumor–immune interaction models can be summarized as follows:

(1) The proposed model extends the classical tumor–immune frameworks developed by De Pillis et al. by incorporating macrophage polarization dynamics, cytokine-mediated regulation, and immune-strength-dependent tumor–immune interactions within a unified chemo-immunotherapy framework. Unlike the original De Pillis models, the proposed formulation explicitly accounts for both anti-tumor (M1) and pro-tumor (M2) macrophage phenotypes as well as the positive and negative feedback loops generated by cytokines and immune-cell interactions. Recent studies have highlighted the importance of macrophage plasticity and tumor microenvironment regulation in determining cancer progression and treatment response. Building on these findings, the proposed model investigates how macrophage polarization, cytokine signaling, and immune regulation collectively influence tumor dynamics. Furthermore, to reduce computational complexity while preserving the dominant biological mechanisms, a reduced-order model is derived using quasi-steady-state approximations for cytokine concentrations.

(2) A comprehensive mathematical and computational analysis of the model is performed to identify the dominant mechanisms governing tumor progression. In addition to proving the non-negativity of solutions and analyzing the existence and stability of tumor-free and cancerous equilibrium points, both local and global sensitivity analyses are conducted. The results reveal that, besides classical tumor-growth parameters, the parameters associated with immune-system strength are among the most influential factors affecting tumor evolution. These findings provide quantitative evidence regarding the critical role of immune competence, macrophage-mediated regulation, and cytokine feedback mechanisms in shaping treatment outcomes.

(3) The proposed framework is further utilized to investigate the effectiveness of chemotherapy, immunotherapy, and combined chemo-immunotherapy under different initial tumor burdens and immune-system conditions. The simulations demonstrate that treatment efficacy strongly depends on both tumor size and host immune competence. In particular, the results indicate that chemotherapy or immunotherapy alone may be insufficient in certain scenarios,

ACCEPTED MANUSCRIPT

whereas combined chemo-immunotherapy can significantly improve tumor control. These findings provide mechanistic insight into the conditions under which combination therapies become necessary and highlight the potential value of integrating immune-system characteristics into treatment-design strategies.

To sum up, the present work has the following novelties:

- Integration of macrophage polarization, cytokine feedback loops, immune-strength dynamics, and chemo-immunotherapy in a single framework.
- Reduced-order formulation using quasi-steady-state approximation while preserving key immune mechanisms.
- Combined local/global sensitivity analysis identifying immune-strength parameters as dominant determinants of outcomes.
- Treatment-strategy comparison across different tumor burdens and immune conditions.
- Coupling patient immune competence with treatment response, which provides a bridge between tumor dynamics and personalized therapy design.

The organization of the paper is as follows. The mathematical model is presented in Section 2. The positivity of the solutions, sensitivity analysis, deriving the equilibrium points, and stability analysis are examined in Section 3. In Section 4, different treatment strategies are studied. Finally, the conclusion is presented in Section 5.

2. Mathematical model

- The target of the proposed model is to study the tumor growth in dealing with the immune system by considering macrophage polarization and cytokine dynamics. The model is the extension of the proposal of De Pillis et. al [50] with the addition of macrophages polarization and cytokine dynamics. Our model added the effect of IL6, IL10, IL12, TGF-β, Regulatory T cells (Regulatory T cells (Tregs)), Th1, M1, and M2 to the De Pillis et. al models. So, the states of the system are:
- $T(t)$, tumor cells population,
- $N(t)$, natural killer cells population,
- $L(t)$, CD8+ T cells population,
- $C(t)$, circulating lymphocytes not including NK cells, CD8+ T cells or regulatory T cells,
- $T_1(t)$, Type-1 helper T-cells population,
- $R(t)$, regulatory T cells (Regulatory T cells (Regulatory T cells (Tregs))) population,
- $M_1(t)$, the density of pro-inflammatory tumor associated macrophages M_1,
- $M_2(t)$, the density of anti-inflammatory tumor associated macrophages M_2,
- $I_2(t)$, IL2 concentration,
- T_β, TGF-β concentration,
- $I_6(t)$, IL6 concentration,
- $I_{10}(t)$, IL10 concentration,
- $I_{12}(t)$, IL12 concentration,
- $M(t)$, chemo-drug concentration in the blood stream.

Remark1. In this work, the functional forms of each cell interactions are discussed: (1) the product form is used to show the interactions between cells, namely, αAB, where A and B are populations of cells and α is a constant; (2) the

ACCEPTED MANUSCRIPT

interaction of cells with cytokines are regarded as a Michaelis–Menten form, i.e. $pIC/(g+I)$, where I is the cytokine's concentration, C is the population of cell, and p, g are constant. They are widely accepted and used models [43].

The following general assumptions have been considered in modeling:

- Logistic growth of tumor cells when there is no immune response. It is based on curve fitting on clinical data [45].
- The tumor cell killing ability for both NK and CD8+ T cells
- Increasing and expanding cytolytic activity by both NK and CD8+ T cells
- NK cells show the innate immune response
- CD8+ T cells show the adaptive immune response
- Both NK and CD8+ T cells are deactivated in dealing with tumor cells
- The population of circulating lymphocytes shows the level of patient health
- Chemo-drug kills both normal and tumor cells

Other assumptions are presented in the derivation of each ODE's term.

2.1. Full model

We developed a detailed model considering cytokine dynamics and cell dynamics. We use ordinary differential equations to describe the growth and the death of each agent and its interaction with other agents. Fig. 1 demonstrates detailed interactions of immune cells with each other and with tumor cells. The dynamics of each state are described as follows:

1) Tumor cells:

It is regarded that the tumor grows logistically in the absence of immune cells [45]. The contribution of NK-cell-mediated tumor-cell elimination is incorporated into the model through the term $-ce^{-\lambda_T R}NT$ The term $e^{-\lambda_T R}$ shows the immunosuppression effect of regulatory T cells [46]. The interaction between tumor cells and M1 and Th1 is also added in the product form [44].

$$dT/dt = aT(1-bT) - ce^{-\lambda_T R}NT - DT - \delta_{m_1} M_1 T - \delta_{T_1} T_1 T \quad (1)$$

Where, *D* shows the patient's immune strength.

2) **Natural killer cells:**

The natural killer cells are produced from circulating lymphocytes (term eC). They die naturally with the rate f and inactivated due to "antibody-dependent cell-mediated cytotoxicity" (ADCC). NK cells induced term due to the presence of IL2 is presented in a Michaelis–Menten form [38, 39].

$$dN/dt = eC - fN + p_N N I_2/(g_N + I_2) \quad (2)$$

3) CD8+ T cells:

The cytotoxic T lymphocytes (CTL) turnover, which is inhibited by IL2, is shown by $\theta mL/(\theta + I_2)$. The parameter θ shows original meaning of m. The term qLT shows the cytolytic potential. Recruitment of CTL by debris of tumor cells lysed by natural killer cells is shown by $r_1 NT$. The activation of naïve CD8+ T cells in the general lymphocyte population is shown by the term $r_2 CT$. Moreover, CTL is activated by IL-2 which shows by the term $\beta_2 I_2 L/(k_2 + I_2)$. The term $jTL/(k+T)$ shows the accumulation of effector cells via CTL stimulation. The breakdown of surplus CTLs in the presence of Regulatory T cells (Tregs) is shown by the term $uL^2 R I_2/(k_k + I_2)$.

ACCEPTED MANUSCRIPT

$$dL/dt = -\theta mL/(\theta + I_2) + (\beta_2 I_2 L)/(k_2 + I_2) + jTL/(k + T) + (r_1 N + r_2 C)T - (uL^2 RI_2)/(k_k + I_2) - qLT \quad (3)$$

4) Lymphocytes:

One of the most important parameter should be considered is the population of lymphocytes. This population estimates the level of the immune system's strength. It is assumed that lymphocytes are produced in bone marrow with rate α and their turnover rate is regarded as βC.

$$dC/dt = \alpha - \beta C \quad (4)$$

5) Interleukins-2:

Interleukin-2 is produced by Regulatory T cells (Tregs) and naïve CTLs which is shown by the term ϕC. The term $\omega LI_2/(\xi + I_2)$ shows the production of IL2 by activated CTLs. The term $-\mu_{I_2} I_2$ shows the natural death [39]. The effect of Th1 cells in production of IL2 is also added by the term $\lambda_{I_2 T_1} T_1$.

$$dI_2/dt = -\mu_{I_2} I_2 + \phi C + \omega LI_2/(\xi + I_2) + \lambda_{I_2 T_1} T_1 \quad (5)$$

6) T helper cells:

Pro-inflammatory M1 macrophages associated with the tumor microenvironment can modulate the population of helper T lymphocytes, with a particularly pronounced influence on the Th1 subset. This interaction is incorporated into the model through the term $\lambda_{T_1 M_1} T_0 M_1/(M_1 + K_{M_1})$. The secretion mechanisms assumed for IL-2 and IL-12 are represented using analogous functional expressions. In contrast, IL-10 exerts an opposing regulatory effect relative to IL-12. The spontaneous loss of Th1 cells is described by the corresponding natural mortality term $-d_{T_1} T_1$. Accordingly, the temporal evolution of the Th1-cell population can be formulated as follows [19]:

$$\frac{dT_1}{dt} = \lambda_{T_1 M_1} T_0 \frac{M_1}{M_1 + K_{M_1}} \left(\frac{I_{12}}{I_{12} + K_{I_{12}}}\right)\left(\frac{K_{I_{10}}}{K_{I_{10}} + I_{10}}\right) + \lambda_{TI_2}\left(\frac{I_2}{I_2 + K_{I_2}}\right) T_1 - d_{T_1} T_1 \quad (6)$$

7) Regulatory T Cells:

The production term of Regulatory T cells (Tregs) is wC, and the turnover term is $-u_R R$. The IL2 induced proliferation term is $(p_R RI_2/(g_R + I_2))(T_\beta/(T_\beta + g_{T_\beta}))$, where the Hill-type formulation $T_\beta/(T_\beta + g_{T_\beta})$ describes the concentration-dependent activation of regulatory T cells, with the parameter g_{T_β} corresponding to the concentration required to achieve half-maximal activation by TGF-β. In addition, TGF-β-mediated signaling promotes the differentiation of Th0 cells into the regulatory T-cell phenotype. This differentiation process is incorporated into the model through the term $\lambda_{T_{reg}} T_0 T_\beta/(T_\beta + K_{T_\beta})$.

$$\frac{dR}{dt} = wC - u_R R + \left(\frac{p_R RI_2}{g_R + I_2}\right)\left(\frac{T_\beta}{T_\beta + g_{T_\beta}}\right) + \lambda_{T_{reg}} T_0 \left(\frac{T_\beta}{T_\beta + K_{T_\beta}}\right) \quad (7)$$

8) Macrophages:

Macrophages have a significant effect on tumor growth [47] and treatment response [48]. Apoptosis and switch type are two possible ways to attract the macrophages to the tumor site [49]. TGF-β and IL6 cause the transition between macrophages. The following equations show the dynamics of the macrophages:

ACCEPTED MANUSCRIPT

$$\frac{dM_1}{dt} = s_1 - K_1 M_1 + \nu M_2 - \left(\lambda_1 T_\beta + \lambda_2 I_6\right) M_1 \tag{8}$$

$$\frac{dM_2}{dt} = s_2 + \left(\lambda_1 T_\beta + \lambda_2 I_6\right) M_1 - K_2 M_2 - \nu M_2 \tag{9}$$

Here, the parameters s_1 and s_2 denote the respective influx terms for the M1 and M2 macrophage populations, whereas K_1 and K_2 characterize their corresponding natural depletion rates. The phenotypic switching between the two macrophage states is modeled as a function of the concentrations of TGF-β and IL-6.

9) Cytokines:

It is regarded that the cytokines are produced at a constant rate by corresponding cells. Moreover, their death is also assumed to be at a constant rate [43, 49]. So we have:

$$\frac{dT_\beta}{dt} = \alpha_1 T - d_1 T_\beta \tag{10}$$

$$\frac{dI_6}{dt} = \alpha_6 T - d_6 I_6 \tag{11}$$

$$\frac{dI_{10}}{dt} = \alpha_{10} M_2 - d_{10} I_{10} \tag{12}$$

$$\frac{dI_{12}}{dt} = \alpha_{12} M_1 - d_{12} I_{12} \tag{13}$$

The quantities $\alpha_1, \alpha_6, \alpha_{10}$, and α_{12} represent the respective synthesis rates, whereas d_1, d_6, d_{10}, d_{12} denote the corresponding removal or degradation coefficients. All these parameters in Eqs. (10)-(13) will be estimated by clinical data.

10) Chemotherapy and immunotherapy:

It is assumed that the chemo-drug will be removed through time at a rate proportional to its concentration. This is shown as an exponential decay term, $-\gamma_M M$:

$$\frac{dM}{dt} = -\gamma_M M + \nu_M\left(t\right) \tag{14}$$

The dose of chemotherapy is shown by $\nu_M\left(t\right)$. The effect of chemotherapy on each cell population is shown by the term $-K_\phi\left(1-e^{-\delta_\phi M}\right)\phi$

The direct injections of antigen-specific CTL cells and IL-2 are shown by the terms $\nu_L\left(t\right)$ and $\nu_{I_2}\left(t\right)$, respectively [38].

11) Patient immune strength relation:

The expression below is introduced to quantify the antitumor activity of cytotoxic T lymphocytes and is referred to as immune strength [39]. Its formulation incorporates both the lymphocyte population, denoted by L and the overall tumor burden, represented by T .

$$D = d\,\frac{\left(L/T\right)^l}{s + \left(L/T\right)^l} \tag{15}$$

ACCEPTED MANUSCRIPT

Variations in the parameters s, l and d, lead to distinct levels of immune strength within the model.

It has to be noted that Immune-cell proliferation is incorporated implicitly through activation, recruitment, differentiation, and cytokine-mediated expansion terms appearing in Eqs. (1)–(15). The model therefore captures the net population-level growth of immune cells without explicitly representing intracellular cell-cycle dynamics.

2.2. Reduced order model

For the cytokine concentrations, a quasi-steady-state assumption is adopted, such that their temporal variations are considered sufficiently small and can be neglected [43, 49]. The production and decay of cytokines occur on a very short timescale in comparison with cancer cells and CTL cells. Under this assumption, Eqs. (10) – (13) are simplified as follows:

$$T_\beta = \frac{\alpha_1}{d_1} T \tag{16}$$

$$I_6 = \frac{\alpha_6}{d_6} T \tag{17}$$

$$I_{10} = \frac{\alpha_{10}}{d_{10}} M_2 \tag{18}$$

$$I_{12} = \frac{\alpha_{12}}{d_{12}} M_1 \tag{19}$$

Substituting (16)-(19) into Eqs. (1)-(9), the following simplified system is obtained for cell dynamics:

$$\frac{dT}{dt} = aT\left(1-bT\right) - ce^{-\lambda_T R} NT - DT - \delta_{m_1} M_1 T - \delta_{T_1} T_1 T - K_T\left(1-e^{-\delta_T M}\right)T \tag{20}$$

$$\frac{dN}{dt} = eC - fN - pNT + \frac{p_N N I_2}{g_N + I_2} - K_N\left(1-e^{-\delta_N M}\right)N \tag{21}$$

$$\frac{dL}{dt} = -\frac{\theta m L}{\theta + I_2} + \frac{\beta_2 I_2 L}{k_2 + I_2} + \frac{jTL}{k+T} + \left(r_1 N + r_2 C\right)T - \frac{uL^2 R I_2}{k_k + I_2} - qLT - K_L\left(1-e^{-\delta_L M}\right)L + \nu_L(t) \tag{22}$$

$$\frac{dC}{dt} = \alpha - \beta C - K_C\left(1-e^{-\delta_C M}\right)C \tag{23}$$

$$\frac{dI_2}{dt} = -\mu_{I_2} I_2 + \phi C + \frac{\omega L I_2}{\xi + I_2} + \lambda_{I_2 T_1} T_1 + \nu_{I_2}(t) \tag{24}$$

$$\frac{dT_1}{dt} = \lambda_{T_1 M_1} T_0 \frac{M_1}{M_1 + K_{M_1}}\left(\frac{\gamma_1 M_1}{\gamma_1 M_1 + K_{I_{12}}}\right)\left(\frac{K_{I_{10}}}{K_{I_{10}} + \gamma_2 M_2}\right) + \lambda_{TI_2}\left(\frac{I_2}{I_2 + K_{I_2}}\right)T_1 - d_{T_1} T_1 - K_{T_1}\left(1-e^{-\delta_{T_1} M}\right)T_1 \tag{25}$$

$$\frac{dR}{dt} = wC - u_R R + \left(\frac{p_R R I_2}{g_R + I_2}\right)\left(\frac{\gamma_3 T}{\gamma_3 T + g_{T_\beta}}\right) + \lambda_{T_{reg}} T_0\left(\frac{\gamma_3 T}{\gamma_3 T + K_{T_\beta}}\right) - K_R\left(1-e^{-\delta_R M}\right)R \tag{26}$$

$$\frac{dM_1}{dt} = s_1 - K_1 M_1 + \nu M_2 - \left(\lambda_1\gamma_3 + \lambda_2\gamma_4\right)TM_1 - K_{M_1}\left(1-e^{-\delta_{M_1} M}\right)M_1 \tag{27}$$

$$\frac{dM_2}{dt} = s_2 + \left(\lambda_1\gamma_3 + \lambda_2\gamma_4\right)TM_1 - K_2 M_2 - \nu M_2 - K_{M_2}\left(1-e^{-\delta_{M_2} M}\right)M_2 \tag{28}$$

ACCEPTED MANUSCRIPT

$$\frac{dM}{dt} = -\gamma_M M + v_M(t) \tag{29}$$

Where $\gamma_1 = \alpha_{12} / d_{12}, \gamma_2 = \alpha_{10} / d_{10}$, and $\gamma_4 = \alpha_6 / d_6$. The description of each parameter used in the model, units, their values, and reference sources are shown in Table 2. These parameters have been extracted from curve fitting on human clinical trials. The parameter values were adopted from previously published studies, where they were estimated through curve-fitting procedures using experimental and/or clinical data. The corresponding references are provided in Table 2.

Table 2: parameters of the system, their values and units [19, 38, 39, 45]

parameter	units	value	Description
a	day^{-1}	4.31×10^{-1}	Growth rate of tumor
b	cells^{-1}	1.02×10^{-9}	Inverse of carrying capacity
c	cells^{-1}day^{-1}	2.9077×10^{-13}	Rate of NK-induced tumor death
d	day^{-1}	1.88	Immune system strength coefficient
l	None	1.81	Immune system strength coefficient
s	None	3.5×10^{-2}	Immune system strength coefficient
λ_T	L cell^{-1}	1.59×10^{-9}	Suppressive effect of Regulatory T cells (Regulatory T cells (Tregs)) on tumor cell kill rate by NK cells
δ_{m_1}	L cell^{-1} day^{-1}	1×10^{-9}	Death rate of cancer cells by M1 macrophages
δ_{T_1}	L cell^{-1} day^{-1}	1×10^{-9}	Death rate of cancer cells by Th1 cells
K_T	day^{-1}	9×10^{-1}	Death rate of tumor cells due to chemotherapy
δ_T	L mg^{-1}	1.8328	Chemotherapy efficacy coefficient on cancer cells
f	day^{-1}	1.25×10^{-2}	Rate of NK cell turnover
e	day^{-1}	f / 9	Rate of NK synthesis from circulating lymphocytes
p	cells^{-1}per day^{-1}	2.794×10^{-13}	Rate of NK cell death due to tumor interaction
p_N	day^{-1}	6.68×10^{-2}	Rate of IL-2 induced NK cell proliferation
g_N	IU/1^{-1}	2.5036×10^{5}	Concentration of IL-2 for half-maximal NK cell proliferation
K_N	day^{-1}	6.75×10^{-2}	Rate of NK cell depletion due to chemotherapy toxicity
δ_N	L mg^{-1}	1.8328	Coefficient of chemotherapy toxicity on NK cells
θ	IU L^{-1}	2.5036×10^{-3}	Concentration of IL-2 to halve CD8+ T cell turnover
m	day^{-1}	9×10^{-3}	Rate of activated CD8+ T cell turnover
u	L^2 cell^{-2}day^{-1}	4.417×10^{-14}	CD8+ T cell self-limitation feedback coefficient
k_k	IU L^{-1}	2.5036×10^{3}	Concentration of IL-2 to halve magnitude of CD8+ T cell self-regulation
β_2	Pg/cell day	2.4036	Rate of IL-2 induced CD8+ T cell activation
k_2	Pg/ml	2.5036×10^{3}	Concentration of IL-2 for half-maximal CD8+ T cell activation
j	day^{-1}	1.245×10^{-1}	Rate of CD8+ T-lysed tumor cell debris activation of CD8+ T cell
k	IU/1^{-1}	2.019×10^{7}	Tumor size for half-maximal CD8+ T-lysed debris CD8+ T activation

ACCEPTED MANUSCRIPT

r_1	cells^{-1}per day^{-1}	2.9077×10^{-11}	Rate of NK-lysed tumor cell debris activation of CD8+ T cells
r_2	cells^{-1}per day^{-1}	5.8467×10^{-13}	Rate of CD8+ T cell production from circulating lymphocytes
q	cells^{-1}per day^{-1}	3.422×10^{-10}	Rate of CD8+ T cell death due to tumor interaction
k_L	day^{-1}	4.86×10^{-2}	Rate of CD8+ T cell depletion from chemotherapy toxicity
δ_L	L mg^{-1}	1.8328	Coefficient of chemotherapy toxicity on CD8+ T cell
α	cells L^{-1} day^{-1}	$3*10^9*\beta$	Rate of circulating lymphocyte production
β	day^{-1}	6.3×10^{-3}	Rate of circulating lymphocyte turnover
K_C	day^{-1}	3.4×10^{-2}	Rate of lymphocyte depletion from chemotherapy toxicity
δ_C	L mg^{-1}	1.8328	Coefficient of chemotherapy toxicity on circulating lymphocytes
μ_{I_2}	day^{-1}	11.7427	Rate of excretion and elimination of IL-2
ϕ	IU/cells^{-1}per day^{-1}	2.38405×10^{-7}	Rate of IL-2 production from CD4+/naive CD8+ T cell
ω	IU/cells^{-1}per day^{-1}	7.874×10^{-2}	Rate of IL-2 production from CD8+ T cell
ξ	IU/1^{-1}	2.5036×10^{3}	Concentration of IL-2 for half-maximal CD8+ T cell IL-2 production
$\lambda_{I_2T_1}$	IU cell^{-1} day^{-1}	0.0672	Production rate of IL-2 by th1 cells
$\lambda_{T_LM_L}$	day^{-1}	0.23	Production rate of Th1 cells by M1 macrophages and IL-12
T_0	cells L^{-1}	2×10^{10}	Constant source of naïve T cells
k_{M_1}	cells L^{-1}	5×10^{10}	M1 saturation
$k_{I_{12}}$	IU L^{-1}	1.95×10^{8}	IL-12 saturation
$k_{I_{10}}$	IU L^{-1}	3×10^{4}	IL-10 saturation
λ_{TI_2}	day^{-1}	1	Production rate of Th1 cells by IL-2
k_{I_2}	IU L^{-1}	8×10^{6}	IL-2 saturation
d_{T_1}	day^{-1}	1.97×10^{-1}	Death rate of Th1 cells
K_{T_1}	cells L^{-1}	3.4×10^{-2}	Rate of Th1 depletion from chemotherapy toxicity
δ_{T_1}	L cell^{-1} day^{-1}	1.8328	Coefficient of chemotherapy toxicity on Th1
w	day^{-1}	4.698×10^{-4}	Rate of Treg cell production from circulating lymphocytes
u_R	day^{-1}	3.851×10^{-2}	Rate of Treg cell turnover
p_R	day^{-1}	3.598×10^{-2}	Rate of IL-2-induced Treg cell proliferation
g_R	IU L^{-1}	11.027	Concentration of IL-2 necessary for half-maximal activation of Regulatory T cells (Regulatory T cells (Tregs))
g_{T_β}	IU L^{-1}	7×10^{4}	Concentration of TGF-β for half-maximal activation of Regulatory T cells (Tregs)
$\lambda_{T_{reg}}$	day^{-1}	0.001	Production rate of Regulatory T cells (Tregs) from Th0 cells due to TGF-β
k_{T_β}	IU L^{-1}	2600	TGF-β saturation
K_R	cells L^{-1}	3.4×10^{-2}	Rate of Treg cell depletion from chemotherapy toxicity

ACCEPTED MANUSCRIPT

δ_R	L mg^{-1}	1.8328	Chemotherapy toxicity on Regulatory T cells (Tregs)
s_1	day^{-1}	40	Influx rate of M1
K_1	day^{-1}	0.02	DEath rate of M1
ν	day^{-1}	5×10^{-2}	Transition rate from M2 to M1
λ_1	day^{-1}	0.075	Transition rate from M1 to M2 depend on TGF-β
λ_2	day^{-1}	0.075	Transition rate from M1 to M2 depend on IL-6
K_{M_1}	cells L^{-1}	0.6	Rate of M1 depletion from chemotherapy toxicity
δ_{M_1}	L mg^{-1}	1.8328	Coefficient of chemotherapy toxicity on M1
s_2	day^{-1}	20	flux rate of M2
K_2	day^{-1}	8×10^{-3}	Death rate of M2
K_{M_2}	cells L^{-1}	0.6	Rate of M2 depletion from chemotherapy toxicity
δ_{M_2}	L mg^{-1}	1.8328	Coefficient of chemotherapy toxicity on M2
α_1	Pg/cell day	7×10^{-4}	Production rate of TGF-β
d_1	day^{-1}	10	Death rate of TGF-β
α_6	Pg/cell day	7×10^{-5}	Production rate of IL-6
d_6	day^{-1}	0.173	Death rate of IL-6
α_{10}	Pg/cell day	5×10^{-4}	Production rate of IL-10
d_{10}	day^{-1}	5	Death rate of IL-10
α_{12}	Pg/cell day	3×10^{-2}	Production rate of IL-12
d_{12}	day^{-1}	1.188	Death rate of IL-12
γ_M	day^{-1}	4.077×10^{-1}	Rate of excretion and elimination of chemotherapy drug

3. Dynamics analysis of the model

3.1. Positivity of the solutions:

Lemma 1: Suppose $\dot{\psi}(t)=\chi_1(t)-\chi_2(t)\psi(t)$ is a first order ODE, where $\chi_1(t):\mathbb{R}\to\mathbb{R}^+$ and $\chi_2(t):\mathbb{R}\to\mathbb{R}$. The solution $\psi(t)$ is in variant in $\Re^+$.

Proof: Suppose $\psi(0)\geq 0\in\mathbb{R}^+$ The solution $\psi(t)$ is:

$$\psi(t)=\psi(0)e^{-\int_0^t\chi_2(s)\,ds}+e^{-\int_0^t\chi_2(s)\,ds}\int_0^t\chi_1(\tilde{t})\;e^{\int_0^{\tilde{t}}\chi_2(s)\,ds}d\tilde{t}\,. \tag{30}$$

Under the condition $\chi_1(t)\geq 0$, we obtain the inequality $\psi(t)\geq 0$. Therefore, for every strictly positive initial state satisfying $\psi(0)\geq 0$, the corresponding trajectory cannot leave the admissible region $\mathbb{R}^+$. Thus, the solution remains within this set for all subsequent times, demonstrating the invariance of $\psi(t)$. ■

ACCEPTED MANUSCRIPT

The non-negativity of all state variables in the proposed cancer model follows from Lemma 1, which establishes the positivity of the corresponding solutions.

Theorem 1: Given the initial conditions $T \geq 0, N \geq 0, L \geq 0, C \geq 0, I_2 \geq 0, T_1 \geq 0, R \geq 0, M_1 \geq 0$ and $M_2 \geq 0$, then the solutions of states, in the absence of the treatment, remain positive for all $t \geq 0$. In other words, For the untreated formulation, every trajectory generated by Eqs. (20)–(28) remains confined to the non-negative portion of the state space associated with the free system.

Proof: The plane $T = 0$ is an invariant plane, because the state T is a common term in Eq. (20). In other words, when the trajectory of the system reaches to $T = 0$ we have $\frac{dT}{dt} = 0$. Hence, if $T(0) \geq 0$ implies that $T(t)$ remains non-negative.

The macrophages dynamics gives:

$$\frac{dM_1(t)}{dt} \geq s_1 - K_1 M_1(t) - (\lambda_1\gamma_3 + \lambda_2\gamma_4) T(t) M_1(t) = s_1 - \left(K_1 + (\lambda_1\gamma_3 + \lambda_2\gamma_4) T(t)\right) M_1(t) \tag{31}$$
$$= \varrho_1(t) - \varrho_2(t) M_1(t)$$

where $\varrho_1(t) \geq 0$. Similarly,

$$\frac{dM_2(t)}{dt} \geq s_2 - K_2 M_2(t) - \nu M_2(t) = s_2 - (K_2 + \nu) M_2(t) = \omega_1(t) - \omega_2(t) M_2(t) \tag{32}$$

Where $\omega_1(t) \geq 0$. Both non-equalities satisfy the conditions of Lemma 1. Hence, $M_1(t), M_2(t) \geq 0$. Considering the circulating lymphocytes' dynamics implies:

$$\frac{dC(t)}{dt} \geq -\beta C(t) \Rightarrow C(t) \geq C(0) e^{-\beta t} \geq 0 \tag{33}$$

Regarding T-helper cells' dynamics implies:

$$\frac{dT_1}{dt} \geq \lambda_{TI_2} \left(\frac{I_2(t)}{I_2(t) + K_{I_2}} \right) T_1(t) - d_{T_1} T_1(t) = 0 - \left(d_{T_1} - \lambda_{TI_2} \left(\frac{I_2(t)}{I_2(t) + K_{I_2}} \right) \right) T_1(t) \tag{34}$$
$$= \eta_1(t) - \eta_2(t) T_1(t)$$

where $\eta_1(t) \geq 0$ and the condition of Lemma 1 is satisfied; hence, $T_1(t) \geq 0$.

By approaching the trajectory of the system to the plane $I_2 = 0$ we have:

$$\frac{dI_2(t)}{dt} = \phi C(t) + \lambda_{I_2 T_1} T_1(t) \geq 0. \tag{35}$$

Hence, $I_2(t) \geq 0$ Also,

$$\frac{dN(t)}{dt} \geq -fN(t) - pN(t)T(t) + \frac{p_N N(t) I_2(t)}{g_N + I_2(t)} = 0 - \left(f - pT(t) + \frac{p_N I_2(t)}{g_N + I_2(t)} \right) N(t) \tag{36}$$
$$= \vartheta_1(t) - \vartheta_2(t) N(t)$$

where $\vartheta_1(t) \geq 0$. Hence, $N(t) \geq 0$ based on the Lemma 1.

Furthermore, as the system trajectory approaches the boundary defined by L=0, the following relation is obtained:

ACCEPTED MANUSCRIPT

$$\frac{dL}{dt} = \left(r_1 N + r_2 C\right) T \geq 0 \tag{37}$$

Hence, $L(t) \geq 0$.■

3.2. Sensitivity analysis:

The parameter values adopted in the simulations were obtained from a range of previously published sources. Although these parameters' values vary among different patients, these values are near. A local sensitivity assessment is employed to examine how individual parameters and starting states affect the temporal behavior of the model. The analysis is performed by perturbing one selected quantity at a time, while keeping every other model input unchanged. The initial-state variables are assigned values spanning the intervals reported in Table 3, whereas the model parameters are varied over the corresponding ranges specified in Table 4. For each initial state denoted by q, its value is systematically varied across the interval specified in Table 3 using 20 equally spaced increments.

When q is treated as a system parameter, its value is varied over the interval from $0.1q$ up to $1.9q$ (Table 4). A change in q leads to a change in the tumor growth dynamics (Fig. 2). The tumor population on day 20 is considered because the experimental investigations in [50] show that the carrying capacity is reached after 20 days. Percentage change in tumor population due to changes in q is computed as follow:

$$\Delta X\% = \frac{T(20) - T_{base}(20)}{T_{base}(20)} \times 100 \tag{38}$$

Here, $T_{base}(20)$ denotes the tumor-cell population at the 20th day obtained with the nominal parameter set reported in Table 4, whereas $T(20)$ represents the corresponding tumor-cell population at day 20 after modifying the parameter q.

Moreover, the response time of the system is examined by using the time the tumor grows to half the carrying capacity. This time is measured when the tumor population reaches the half population of the tumor on day 20 (Fig. 2). The percentage change in the time of reaching the half-carrying capacities is calculated as follows:

$$\Delta Y\% = \frac{HT - HT_{base}}{HT_{base}} \times 100 \tag{39}$$

Where, HT_{base} is the time when the population of tumor cells reaches half the carrying capacity considering the baseline parameters presented in Table 4, and HT is the time when the population of tumor cells reaches half the carrying capacity with changes in a parameter or initial conditions.

The change in the tumor size on day 20 and the change in reaching half the carrying capacity due to change in the initial conditions (Section 3.2.1) and the parameter values (Section 3.2.2) are investigated in the following subsections.

ACCEPTED MANUSCRIPT

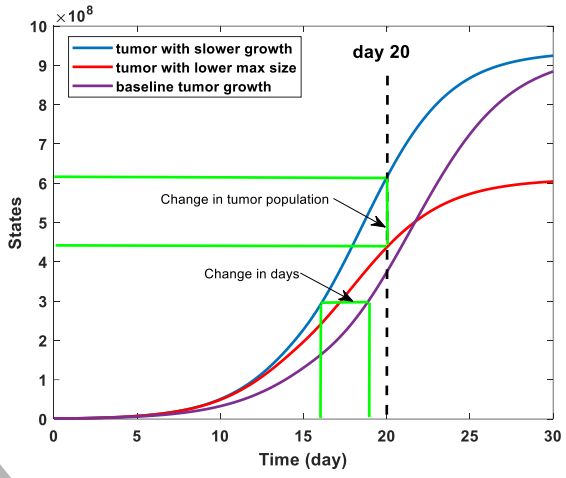


Fig 2: Tumor growth dynamics with baseline parameters and two simulations showing slower tumor growth and tumor growth with lower maximum size. Exemplification to show the change in the tumor population on day 20 and the time to reach half the carrying capacity.

Table 3: The baseline initial conditions and their range of variation (columns 1 and 2). The Max. percentage change in tumor population on day 20 (columns 4 and 6) and its corresponding initial condition (columns 3 and 5).

IC baseline value	Range for IC	IC for max tumor decrease	Max % decrease in tumor	IC for max tumor increase	Max % increase in tumor
$T(0)=10^6$	$(1,10^7)$	1	-100	10^7	15.67
$N(0)=10^3$	$(1,10^5)$	8.4211×10^4	-1.7904×10^{-4}	5.2641×10^3	8.03×10^{-5}
$L(0)=10$	$(1,10^6)$	10^6	-100	1	6.4360×10^{-5}
$C(0)=6\times10^8$	$(1,10^{10})$	10^{10}	-3.5260	1	0.0242
$R(0)=1$	$(1,10^9)$	1	0	10^9	0.0117
$IL2(0)=1073$	$(0,2000)$	1.7895×10^3	-6.178×10^{-5}	526.13	1.4323×10^{-4}
$T1(0)=0$	$(0,10^5)$	10^5	-0.0248	0	0
$M_1(0)=2000$	$(0,10^4)$	1.5789×10^3	-4.4028×10^{-5}	5.2632×10^3	1.4257×10^{-4}
$M_2(0)=2500$	$(0,10^4)$	8.9474×10^3	-3.5694×10^{-5}	8.4211×10^3	3×10^{-4}

ACCEPTED MANUSCRIPT

Table 4: The baseline parameters' value and their range of variation (columns 1 and 2). The Max. percentage change in tumor population on day 20 (columns 4 and 6) and its corresponding initial condition (columns 3 and 5).

Baseline param. values	Simulation range	Param. For max % decrease	max % decrease tumor size	Param. For max % increase	max % increase tumor size
$a = 4.31\times10^{-1}$	$(0.0431, 0.8189)$	0.0431	–99.72	0.8189	17.69
$c = 2.9077\times10^{-13}$	$(2.9077\times10^{-14}, 5.53\times10^{-13})$	5.53×10^{-13}	–0.001271	2.9077×10^{-14}	0.001364
$d = 1.3$	$(0.188, 3.572)$	2.47	–0.02486	0.13	0.02496
$l = 2$	$(0.181, 3.439)$	0.2	–100	3.8	0.02765
$s = 4\times10^{-2}$	$(3.5\times10^{-3}, 6.65\times10^{-2})$	0.004	–0.2504	0.076	0.01308
$b = 1.02\times10^{-9}$	$(1.02\times10^{-10}, 1.938\times10^{-9})$	1.938×10^{-9}	–43.33	1.02×10^{-10}	324.80
$p = 2.794\times10^{-13}$	$(2.794\times10^{-14}, 5.31\times10^{-13})$	1.118×10^{-13}	-6.351×10^{-5}	1.9558×10^{-13}	0.0001162
$p_N = 6.68\times10^{-2}$	$(6.68\times10^{-3}, 12.69\times10^{-2})$	0.1069	-5.805×10^{-5}	0.08684	9.997×10^{-5}
$g_N = 2.5036\times10^{5}$	$(2.5036\times10^{4}, 3.868\times10^{5})$	2.5036×10^{4}	-9.198×10^{-5}	3.254×10^{5}	0.000116
$\alpha_{12} = 3\times10^{-2}$	$(3\times10^{-3}, 5.7\times10^{-2})$	0.03	0	0.057	8.995×10^{-5}
$d_{12} = 1.188$	$(0.1188, 2.2572)$	0.4752	-3.305×10^{-5}	0.8316	0.000106
$\alpha_{10} = 5\times10^{-4}$	$(5\times10^{-5}, 9.5\times10^{-4})$	6.5×10^{-4}	-3.305×10^{-5}	3.5×10^{-4}	0.0001055
$d_{10} = 5$	$(0.5, 9.5)$	3.5	-3.496×10^{-5}	8	0.0001147
$r_1 = 2.9077\times10^{-11}$	$(2.9077\times10^{-12}, 5.524\times10^{-11})$	5.524×10^{-11}	–0.01198	2.9077×10^{-12}	0.011
$r_2 = 5.8467\times10^{-13}$	$(5.8467\times10^{-14}, 11.11\times10^{-13})$	11.11×10^{-13}	–0.02681	5.8467×10^{-14}	0.018255
$\beta_2 = 2.4036$	$(0.24036, 4.567)$	4.566	–0.01607	0.24036	0.006419
$k_2 = 2.5036\times10^{3}$	$(2.5036\times10^{2}, 3.868\times10^{3})$	250.4	–0.04768.	4756.84	0.00356
$j = 1.245\times10^{-1}$	$(1.245\times10^{-2}, 2.3655\times10^{-1})$	0.2365	-0.007176	0.01245	0.00542

ACCEPTED MANUSCRIPT

$k=2.019\times10^{7}$	$(2.019\times10^{6},3.836\times10^{7})$	2.019×10^{6}	-0.002936	3.836×10^{7}	0.001072
$u=4.417\times10^{-14}$	$(4.417\times10^{-15},8.392\times10^{-14})$		-0.3394	8.392×10^{-14}	0.005849
$k_k=2.5036\times10^{3}$	$(2.5036\times10^{2},4.757\times10^{3})$	4.757×10^{3}	-0.006648	2.5036×10^{2}	0.01034
$s_1=40$	$(4,7.6)$	76	-4.084×10^{-5}	16	0.0002434
$v=5\times10^{-2}$	$(5\times10^{-3},9.5\times10^{-2})$	0.02	-4.747×10^{-6}	0.035	0.000155
$K_1=0.02$	$(0.002,0.038)$	0.014	-6.861×10^{-5}	0.008	7.747×10^{-5}
$\lambda_1=0.075$	$(0.0075,0.1425)$	0.0975	-1.153×10^{-5}	0.12	0.000146
$\alpha_1=7\times10^{-4}$	$(7\times10^{-5},13.3\times10^{-4})$	7×10^{-5}	-0.032717	0.00133	0.00231
$d_1=10$	$(1,19)$	19	-0.0036372	1	0.005459
$\lambda_2=0.075$	$(0.0075,0.1425)$	0.0075	-5.457×10^{-5}	0.03	0.000127
$\alpha_6=7\times10^{-5}$	$(7\times10^{-6},13.3\times10^{-5})$	9.1×10^{-5}	-6.443×10^{-5}	11.2×10^{-5}	0.000540
$d_6=0.173$	$(0.0173,0.3287)$	0.3287	-4.422×10^{-5}	0.2768	0.000377
$s_2=20$	$(2,38)$	2	-8.442×10^{-5}	38	4.913×10^{-5}
$K_2=8\times10^{-3}$	$(8\times10^{-4},15.2\times10^{-3})$	0.0032	-6.834×10^{-5}	0.0008	7.328×10^{-5}
$\xi=2.5036\times10^{3}$	$(2.6036\times10^{2},4.757\times10^{3})$	250.36	-0.0258	2503.6	7.777×10^{-5}
$\mu_{I_2}=11.7427$	$(1.1743,22.31)$	1.17427	-0.1298	11.7427	4.57×10^{-5}
$\omega=7.874\times10^{-2}$	$(7.874\times10^{-3},14.96\times10^{-2})$	7.874×10^{-3}	-0.0474	0.10236	0.000264
$\phi=2.38405\times10^{-7}$	$(2.38405\times10^{-8},4.5297\times10^{-7})$	4.53×10^{-7}	-0.001245	2.38×10^{-8}	0.001239
$\theta=2.5036\times10^{-3}$	$(2.5036\times10^{-4},4.757\times10^{-3})$	4.005×10^{-3}	-6.885×10^{-5}	2.5036×10^{-4}	8.3×10^{-5}
$m=9\times10^{-3}$	$(9\times10^{-4},17.1\times10^{-3})$	0.0117	-6.705×10^{-5}	0.0063	8.545×10^{-5}

ACCEPTED MANUSCRIPT

$f=1.25\times10^{-2}$	$(1.25\times10^{-3},2.375\times10^{-2})$	1.25×10^{-3}	-0.0007976	2.375×10^{-2}	0.0007904
$e=1.39\times10^{-3}$	$(1.39\times10^{-4},2.641\times10^{-3})$	2.638×10^{-3}	-0.01322	1.39×10^{-4}	0.012125
$\lambda_{T_1M_1}=0.23$	$(0.023,0.437)$	0.092	-4.714×10^{-5}	0.023	8.403×10^{-5}
$T_0=2\times10^{10}$	$(2\times10^{9},3.8\times10^{10})$	2×10^{9}	-0.2185	3.8×10^{10}	0.006046
$k_{M_1}=5\times10^{10}$	$(5\times10^{9},9.5\times10^{10})$	3.5×10^{10}	-6.64×10^{-5}	5×10^{9}	0.0001114
$k_{I_{12}}=1.95\times10^{8}$	$(1.95\times10^{7},3.705\times10^{8})$	7.8×10^{7}	-3.305×10^{-5}	1.365×10^{8}	0.000106
$k_{I_{10}}=3\times10^{4}$	$(3\times10^{3},5.7\times10^{4})$	21000	-3.5×10^{-5}	48000	0.0001147
$\lambda_{TI_2}=1$	$(0.1,1.9)$	0.7	-6.418×10^{-5}	1.6	0.000121
$\lambda_{I_2T_1}=0.0672$	$(0.00672,0.1277)$	0.047	-3.217×10^{-5}	0.10752	8.728×10^{-5}
$d_{T_1}=1.97\times10^{-1}$	$(1.97\times10^{-2},3.743\times10^{-1})$	0.3743	-2.488×10^{-6}	0.2561	0.000114
$K_{I_2}=8\times10^{6}$	$(8\times10^{5},15.2\times10^{6})$	1.52×10^{7}	-7.054×10^{-5}	1.28×10^{8}	7.24×10^{-5}
$w=4.698\times10^{-4}$	$(4.698\times10^{-5},8.926\times10^{-4})$	4.698×10^{-5}	-0.0003167	8.926×10^{-4}	0.000426
$u_R=3.851\times10^{-2}$	$(3.851\times10^{-3},7.317\times10^{-2})$	7.317×10^{-2}	-0.002173	3.851×10^{-3}	0.00209
$p_R=3.598\times10^{-2}$	$(3.598\times10^{-3},6.836\times10^{-2})$	3.598×10^{-3}	-0.0004096	6.836×10^{-2}	0.000470
$g_R=11.027$	$(1.1027,20.95)$	11.027	5.037×10^{-9}	4.411	0.000122
$g_{T_\beta}=7\times10^{4}$	$(7\times10^{3},13.3\times10^{4})$	$.3\times10^{4}$	-0.0002012	7×10^{3}	0.000878
$\lambda_{T_{reg}}=0.001$	$(0.0001,0.0019)$	0.0001	-0.2185	0.0019	0.006050
$k_{T_\beta}=2600$	$(260,4940)$	4940	-0.0033484	260	0.004937
$\delta_{m_1}=10^{-9}$	$(10^{-9},1.9\times10^{-9})$	10^{-9}	0	1.6×10^{-9}	0.000106
$q=3.422\times10^{-10}$	$(3.422\times10^{-11},6.502\times10^{-10})$	3.422×10^{-11}	-0.002761	6.502×10^{-10}	0.002552

ACCEPTED MANUSCRIPT

$\beta = 6.3\times10^{-3}$	$\left(6.3\times10^{-4}, 11.97\times10^{-3}\right)$	6.3×10^{-4}	–0.00162	11.97×10^{-3}	0.001448
$\alpha = 18.9\times10^{6}$	$\left(18.9\times10^{5}, 35.91\times10^{6}\right)$	35.91×10^{6}	–0.0069706	18.9×10^{5}	0.006667
$\delta_{T_1} = 10^{-9}$	$\left(10^{-10}, 1.9\times10^{-9}\right)$	7×10^{-10}	-4.025×10^{-5}	4×10^{-10}	0.000113
$\lambda_T = 1.59\times10^{-9}$	$\left(1.59\times10^{-10}, 3.021\times10^{-9}\right)$	1.59×10^{-10}	–0.0003556	2.544×10^{-9}	0.000209

3.2.1. Sensitivity to initial conditions

Fig. 3(a) shows the effect of change in initial conditions on the tumor population on day 20. The change in percentage in days to reach half population of the tumor is shown in Fig.3 (b). Each initial condition changes in 20 incremental steps. The range of change of initial conditions is shown in Table 3. As shown in this figure, the initial condition of the adaptive immune system (the initial populations of CD8+ T cells and circulating lymphocytes) has more effects on the final tumor population and on days to reach half-carrying capacity. In other words, the readiness of the immune system against an external object is very important to have a successful treatment. Hence, reinforcing the body facing illness is a key parameter to have a good cure.

The corresponding initial condition for each state causes a maximum and minimum change in the tumor population on day 20 and days to reach half-carrying capacity are shown in Table 3 and Table 5, respectively.

Fig. 3 and Tables 3–5 provide important insights into the role of the initial immune status in determining the subsequent tumor dynamics. The results indicate that the model is particularly sensitive to the initial populations of adaptive immune cells, especially CD8+ T cells and circulating lymphocytes. According to Table 2, increasing the initial CD8+ T-cell population from its baseline value to the upper limit of the investigated range results in a 100% reduction in tumor population on day 20, whereas decreasing this population toward its lower bound produces only a negligible increase in tumor burden. Similar behavior is observed for the initial tumor size. When the initial tumor population is reduced from 10^6 cells to its minimum value, the tumor population on day 20 decreases by approximately 100%, while increasing the initial tumor burden to 10^7 cells increases the final tumor size by approximately 15.67%. These results indicate that the model exhibits strong dependence on the initial balance between tumor burden and immune surveillance.

The response-time analysis shown in Fig. 3(b) and Table 5 further supports this conclusion. Variations in the initial CD8+ T-cell population generate nearly a 100% increase in the time required for the tumor to reach half of its carrying capacity, indicating a substantial delay in tumor progression. In contrast, changes in macrophage populations, IL-2 concentration, and T-helper cells produce only minor changes in both tumor size and response time. This finding suggests that the early adaptive immune response is one of the dominant determinants of disease evolution in the proposed model.

Biologically, these results imply that patients with a larger pool of available effector lymphocytes possess a greater capacity to mount an effective anti-tumor response during the early stages of disease progression. Similar observations have been reported in the tumor–immune interaction models of De Pillis et al. [37], where the initial abundance of immune effector cells strongly influenced the transition between tumor elimination and tumor escape. Therefore, the sensitivity analysis highlights the importance of immune readiness and supports therapeutic strategies aimed at increasing the number or activity of cytotoxic lymphocytes before tumor burden becomes excessive.

3.2.2. Sensitivity to parameters

Fig. 4 illustrates how variations in the model parameters alter the percentage difference in the final tumor-cell population. The corresponding influence of these parameter changes on the time required for the tumor population to decline to one-half of its initial level is presented in Fig. 5.

ACCEPTED MANUSCRIPT

Figs. 4 and 5 present the results of the local sensitivity analysis performed around the nominal parameter set reported in Table 2. For each parameter, the sensitivity measures were calculated by independently varying the parameter within the interval specified in Tables 3–5 while keeping all remaining parameters fixed at their baseline values. Therefore, the results shown in the figures do not correspond to a single parameter value but rather quantify the effect of perturbing each parameter around its nominal operating point. The magnitude of each bar reflects the relative change induced in the selected model output by variations of the corresponding parameter over its prescribed range.

To facilitate interpretation, positive and negative parameter perturbations are displayed separately. The red bars represent the percentage variation in the model output produced when the parameter is increased from its nominal value toward its upper bound, whereas the blue bars represent the corresponding variation when the parameter is decreased toward its lower bound. Consequently, differences between the red and blue bars indicate asymmetry in the model response and reveal nonlinear effects in the underlying tumor–immune interactions. When the red and blue bars have similar magnitudes, the system responds approximately symmetrically to parameter perturbations. In contrast, substantial differences between the two bars suggest that the model is more sensitive to increases or decreases of a particular parameter, reflecting the nonlinear structure of the governing equations.

Figs. 4 and 5 should therefore be interpreted as measures of parameter importance rather than direct simulations of tumor evolution. Fig. 4 quantifies the influence of parameter variations on the tumor population at the selected evaluation time, whereas Fig. 5 illustrates the corresponding effects on the response-time metric used in the study. Together, these figures identify the parameters that exert the greatest control over tumor progression and immune effectiveness. The analysis demonstrates that parameters associated with tumor growth and immune competence has a substantially larger impact on the system dynamics than many of the secondary cytokine-regulation parameters, thereby highlighting the dominant mechanisms governing the behavior of the proposed model.

The sensitivity analysis indicates that the proliferation coefficient a and the carrying capacity b exert a pronounced influence on both the terminal tumor burden and the time required to attain half of the tumor population. Parameter l also produces a substantial variation in these two outcomes. In addition, changes in l modify the quantity D, which characterizes the capacity of the immune response to control and eliminate tumor cells. As expected and mentioned in section 3.2.1, a stronger immune response of the body makes treatment more successful. Diseases such as heart disease, diabetes, and HIV make the immune response weak, and therefore, the treatment strategy may fail. The sensitivity analysis in this paper corresponds with the results obtained in [39] i.e., the proliferation rate a and the parameters l, s and d have more effect on the final population tumor cells.

The influence of the proliferation parameter a and the carrying-capacity parameter b on the system response is further demonstrated in [58].

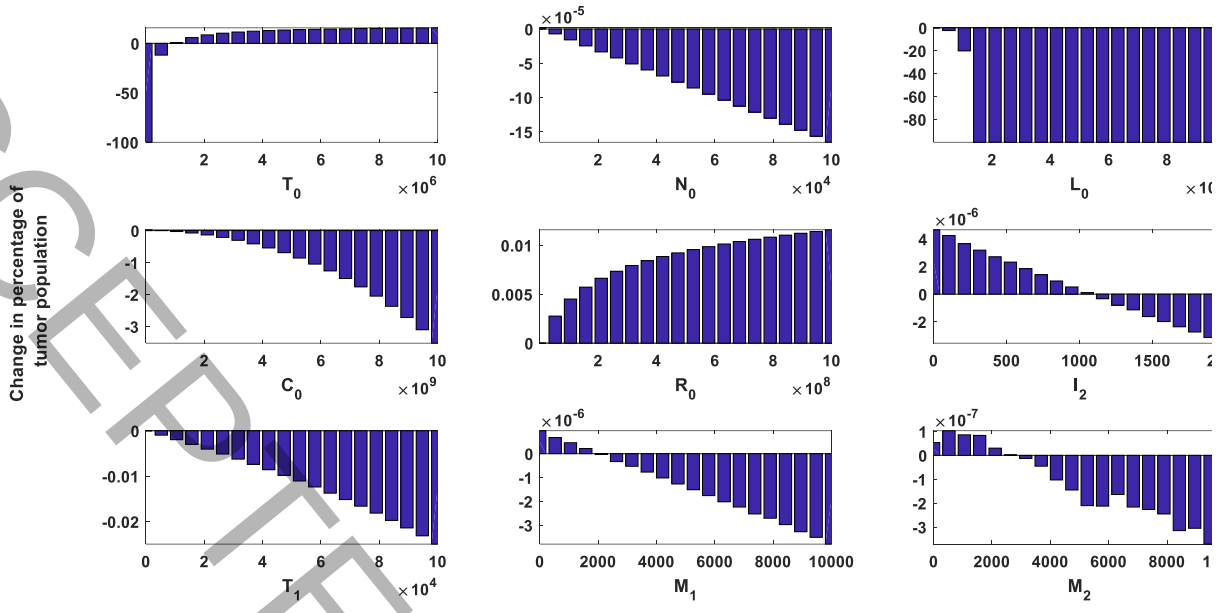
The local sensitivity analysis reveals that only a limited number of parameters exert a dominant influence on tumor progression, whereas most cytokine-related and immune-regulation parameters produce relatively small variations around the baseline solution. As shown in Fig. 4, the tumor proliferation rate (a) is the most influential parameter in the model. Varying (a) within the range reported in Table 3 results in changes in tumor population exceeding 250%, demonstrating that intrinsic tumor growth remains the primary driver of disease progression. This result is consistent with previous tumor–immune models, including the model of De Pillis et al. [38], where tumor proliferation parameters were among the most sensitive quantities governing long-term tumor dynamics. The carrying-capacity parameter (b) also exhibits a strong effect on tumor burden, confirming that environmental constraints and resource limitations substantially affect the final tumor size. Together, parameters (a) and (b) define the intrinsic growth potential of the tumor and therefore determine the baseline level of aggressiveness of the disease. Similar observations have been reported in Ref. [51], where tumor growth parameters dominated the sensitivity ranking.

Among the immune-related parameters, the parameter (l) is particularly noteworthy. Variations of (l) generate changes in tumor burden of the same order of magnitude as some growth-related parameters. Since (l) appears in the immune-strength function (D), it directly regulates the effectiveness of immune-mediated tumor killing. Increasing (l) significantly suppresses tumor growth, whereas decreasing it promotes tumor expansion. The strong sensitivity associated with (l) indicates that the overall competence of the immune system may be as important as intrinsic tumor

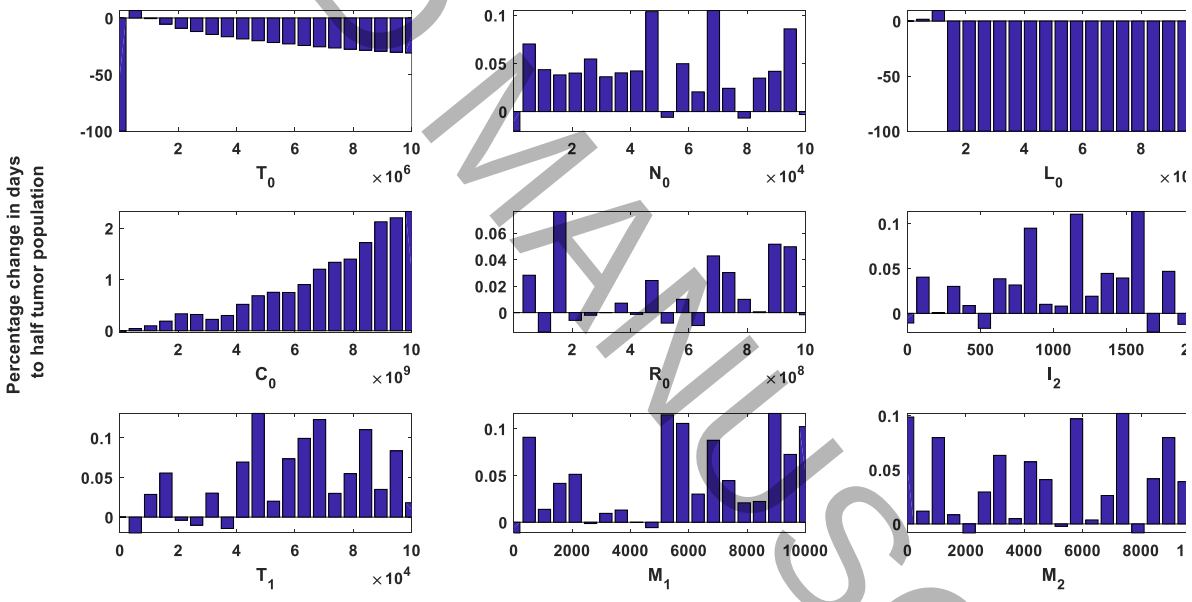
ACCEPTED MANUSCRIPT

characteristics in determining disease outcome. This finding is consistent with the biological observation that immune-compromised patients often exhibit faster tumor progression and poorer treatment outcomes. The remaining immune-strength parameters (s) and (d) also rank among the most influential variables. Although their effects are smaller than those of (a) and (l), Fig. 4 shows that changes in these parameters produce substantially larger variations in tumor population than most cytokine-production and degradation parameters. This result agrees with Ref. [38], where the parameters governing immune effectiveness were identified as key determinants of tumor control. Consequently, the model suggests that enhancing immune competence may shift the balance from tumor persistence toward tumor elimination even when tumor-growth parameters remain unchanged. Fig. 5 provides additional insight through the response-time metric. Parameters (a), (b), and (l) not only affect the final tumor burden but also strongly influence the time required for the tumor to reach half of its carrying capacity. Increasing (a) accelerates tumor progression, whereas increasing (l) delays this process by strengthening immune surveillance. Therefore, these parameters affect both the magnitude and the rate of tumor development. The consistency between Figs. 4 and 5 confirms that tumor progression is governed by a competition between tumor-growth mechanisms and immune-mediated suppression. Parameters associated with cytokine signaling, macrophage polarization, and T-cell regulation generally produce smaller but non-negligible effects, indicating that their primary role is to modulate the effectiveness of the dominant tumor–immune feedback loops rather than directly control tumor growth. This quantitative analysis demonstrates that, in addition to classical tumor-growth parameters, the immune-strength parameters (l), (s), and (d) are among the most influential factors governing cancer dynamics. Therefore, strategies aimed at improving immune competence may provide benefits comparable to those obtained by directly suppressing tumor proliferation, a conclusion that is in agreement with the findings of De Pillis et al. [38] and other tumor–immune interaction studies.

ACCEPTED MANUSCRIPT



(a)



(b)

Fig. 3: (a) Change in percentage of tumor population on day 20; and (b) Change in percentage of days to reach half-carrying capacity; due to change in initial condition in comparison with baseline values. The initial condition of each state is changed in 20 incremental steps in the intervals showed in Table 3.

ACCEPTED MANUSCRIPT

Table 5: The baseline initial conditions and their range of variation (columns 1 and 2). The percentage change in the number of days to reach half tumor population on day 20 (columns 4 and 6) and its corresponding initial condition (columns 3 and 5).

IC baseline value	Range for IC	IC for max day decrease	Max % decrease in day	IC for max day increase	Max % increase in day
$T(0)=10^6$	$(1,10^7)$	1	-100	5.2632×10^5	6.589
$N(0)=10^3$	$(1,10^5)$	1	-0.021	6.842×10^4	0.1048
$L(0)=10$	$(1,10^6)$	10^6	-100	1.0526×10^5	9.545
$C(0)=6\times10^8$	$(1,10^{10})$	1	-0.0227	10^{10}	2.327
$R(0)=1$	$(1,10^9)$	1.053×10^8	-0.0147	1.58×10^8	0.0763
$IL2(0)=1073$	$(0,2000)$	1684	-0.0208	1579	0.1135
$T1(0)=0$	$(0,10^5)$	5.2632×10^3	-0.02	4.737×10^4	0.1309
$M_1(0)=2000$	$(0,10^4)$	0	-0.0115	8.947×10^3	0.1165
$M_2(0)=2500$	$(0,10^4)$	2.105×10^3	-0.0084	7.368×10^3	0.102

ACCEPTED MANUSCRIPT

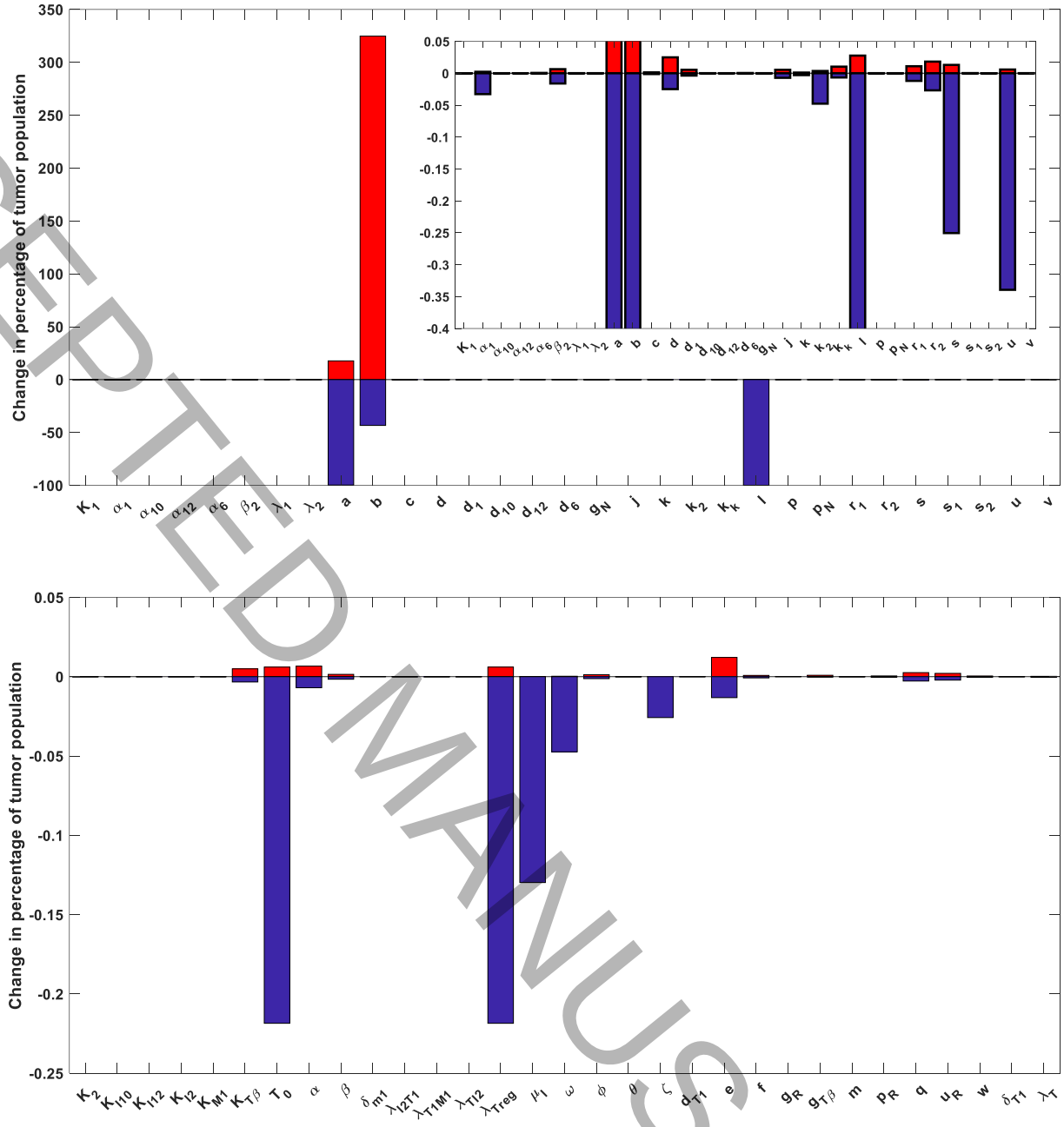


Fig. 4: Change in percentage of tumor population on day 20 due to changes in parameter values from baseline values. The interval for each parameter is presented in Table 4.

The corresponding parameters which cause the maximum and minimum change in tumor population on day 20 are presented in Table 4.

ACCEPTED MANUSCRIPT

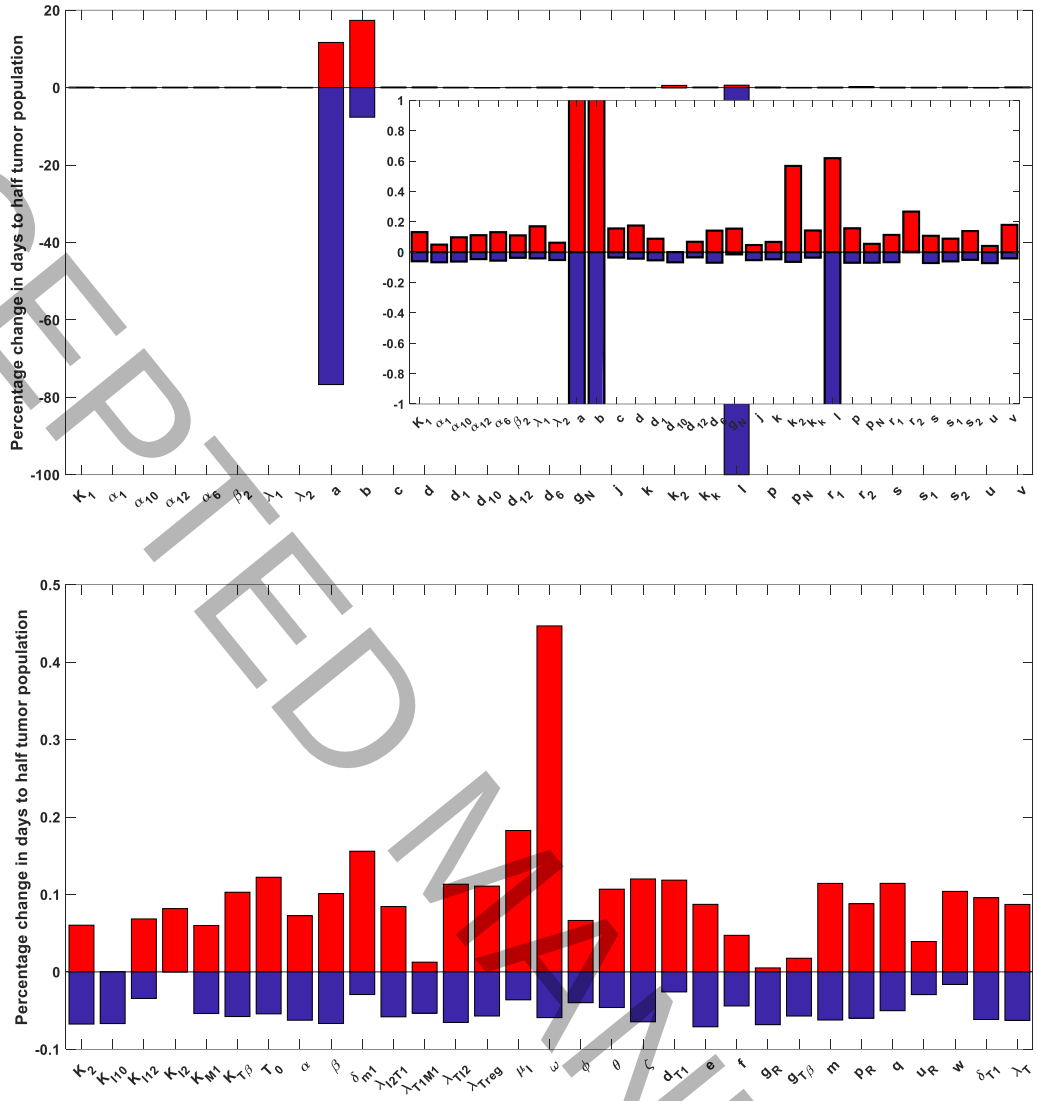


Fig. 5: Change in percentage in number of days to reach the half tumor population on day 20 due to changes in parameter values from baseline values. The interval for each parameter is presented in Table 4.

3.3. Equilibrium points and their stability

The equilibrium points of the system are derived by setting Eqs. (20)-(28), in the absence of the treatment, to zero, and solving them simultaneously:

$$E = \left(T^*, N^*, L^*, C^*, I_2^*, T_1^*, R^*, M_1^*, M_2^*\right) \tag{40}$$

Eq. (23) is decoupled from others. Hence, in all equilibrium points the population of circulating lymphocytes is as follow:

$$C^* = \frac{\alpha}{\beta} \tag{41}$$

The population of tumor cells is computed by setting equation (20) to zero:

$$aT\left(1-bT\right) - ce^{-\lambda_T R}NT - DT - \delta_{m_1} M_1 T - \delta_{T_1} T_1 T = 0 \tag{42}$$

ACCEPTED MANUSCRIPT

Generally, two types of equilibrium points exist in the system. The tumor-free equilibrium points represent the steady states in which there are no tumor cells in the body, i.e. $T = 0$. In the tumor-present equilibrium points, the population of tumor cells is non-zero, which satisfies the following equation:

$$a(1-bT) - ce^{-\lambda_T R}N - D - \delta_{m_1}M_1 - \delta_{T_1}T_1 = 0 \tag{43}$$

Solving Eq. (21) under the steady-state condition yields an expression for the natural killer cell population in terms of the tumor-cell population and:

$$N^* = \frac{eC^*}{f + pT + \dfrac{p_N I_2}{g_N + I_2}} = \Pi(T, I_2) \tag{44}$$

Solving Eq. (26) gives the population of Regulatory T cells (Regulatory T cells (Tregs)) cells as follows:

$$R^* = \frac{wC^* + \lambda_{T_{reg}} T_0 \left(\dfrac{\gamma_3 T}{\gamma_3 T + K_{T_\beta}} \right)}{u_R - \left(\dfrac{p_R I_2}{g_R + I_2} \right) \left(\dfrac{\gamma_3 T}{\gamma_3 T + g_{T_\beta}} \right)} = \Psi(T, I_2) \tag{45}$$

This population is also a function of the tumor-cell and IL-2 populations. By solving the equations related to macrophages populations, i.e. Eqs. (27) and (28), we have:

$$M_1^* = \frac{\varphi_1}{\Delta + \varphi_2 T} \tag{46}$$

$$M_2^* = \frac{\varphi_3 + \varphi_4 T}{\Delta + \varphi_2 T} \tag{47}$$

Where

$$\begin{aligned} \varphi_1 &= (K_1 + v)s_1 + vs_2 \\ \varphi_3 &= K_1 s_2 \\ \Delta &= K_1 (K_2 + v) \end{aligned} \tag{48}$$

Solving Eq. (25) gives the population of the T-helper cells versus the population of tumor cells and interleukins-2. By defining Ω^* as follows:

$$\Omega(T) = \lambda_{T_1 M_1} T_0 \left(\frac{M_1^*}{M_1^* + K_{M_1}} \right) \left(\frac{\gamma_1 M_1^*}{\gamma_1 M_1^* + K_{I_{12}}} \right) \left(\frac{K_{I_{10}}}{K_{I_{10}} + \gamma_2 M_2^*} \right) \tag{49}$$

The population of the T-helper cells is calculated as follows:

$$T_1^* = \frac{\Omega(T)}{d_{T_1} - \lambda_{TI_2} \left(\dfrac{I_2}{I_2 + K_{I_2}} \right)} = \pi(T, I_2) \tag{50}$$

The population of CD8+ T cells is derived by setting Eqs. (22) and (24) to zero. By setting Eq. (24) to zero, the governing equation describing the temporal evolution of the CD8+ T-cell population is formulated as follows:

$$L = \frac{\xi + I_2}{\omega I_2} \left(\mu_{I_2} I_2 - \phi C^* + \lambda_{I_2 T_1} T_1^* \right) = \Sigma(T, I_2) \tag{51}$$

Also, by using Eq. (22), it is concluded that:

ACCEPTED MANUSCRIPT

$$\left(\frac{uRI_2}{k_k+I_2}\right)L^2+\left(qT+\frac{\theta m}{\theta+I_2}-\frac{\beta_2 I_2}{k_2+I_2}-\frac{jT}{k+T}\right)L-\left(r_1N+r_2C\right)T=0 \tag{52}$$

By solving the quadratic Eq. (52), the population of CD8+ T cells is derived as a function of tumor cells and interleukins-2. Moreover, using Eq. (15) gives another equation for deriving the population of CD8+ T cells:

$$L=\left(\frac{DsT^l}{d-D}\right)^{\frac{1}{l}} \tag{53}$$

Where, D is computed by using Eq. (42):

$$D\left(T,I_2\right)=a\left(1-bT\right)-ce^{-\lambda_T R}N^*-\delta_{m_1}M_1^*-\delta_{T_1}T_1^*. \tag{54}$$

Solving the Eqs. (51)-(53) simultaneously gives the population of tumor cells, CD8+ T cells, and IL2. When these three populations are derived, other states in the tumor-present equilibrium points are computed using Eqs. (44)-(50). The intersections of surfaces (51)-(53) show the tumor-present equilibrium points. Fig. 6 shows these intersections using the parameters presented in Table 2.

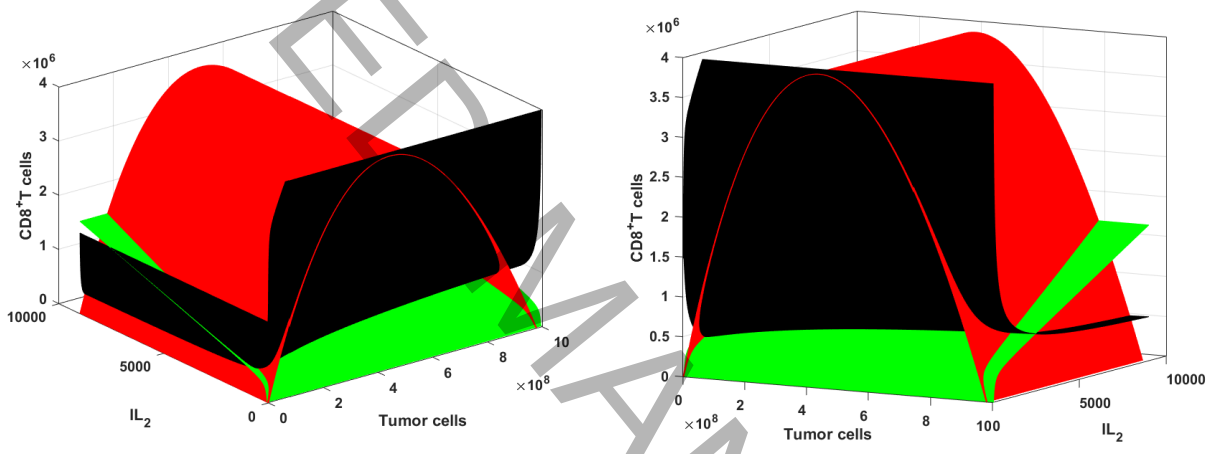


Fig. 6: Tumor-present equilibrium points. The intersections of the Eqs. (51)-(53) from different views.

The tumor-present steady states can be obtained by simultaneously solving Eqs. (51)–(53) while incorporating the relationships defined in Eqs. (44)–(50). For the parameter set listed in Table 2, the analysis reveals two distinct equilibrium states in which tumor cells persist, as illustrated in Fig. 6. The corresponding equilibrium coordinates are reported in Table 6.

ACCEPTED MANUSCRIPT

Table 6: Tumor-bearing equilibrium states determined from the parameter set specified in Table 2.

	T^*	N^*	L^*	C^*	I_2^*	T_1^*	R^*	M_1^*	M_2^*
$E_{TP,1}$	2.4×10^{7}	3.27×10^{8}	4.59×10^{5}	3×10^{9}	850	1.42×10^{-11}	2.46×10^{8}	0.486	7.45×10^{3}
$E_{TP,2}$	9.8×10^{8}	3.45×10^{8}	7.41×10^{5}	3×10^{9}	2.59×10^{3}	8.57×10^{-15}	9.95×10^{8}	0.0119	7.5×10^{3}

According to the formulation introduced in [39], the model admits a single equilibrium state associated with the presence of a tumor. In contrast, the proposed model yields two tumor-present equilibrium points. The tumor-present equilibrium point in Table 6 is similar to the tumor-present equilibrium point in [39], but the population of IL-2 is different.

3.3.1. Tumor-free equilibrium points:

The equilibrium point E_0 related to tumor-free is defined as:

$$E_0 = \left(T_{TF}^*, N_{TF}^*, L_{TF}^*, C_{TF}^*, I_{2TF}^*, T_{1TF}^*, R_{TF}^*, M_{1TF}^*, M_{2TF}^*\right). \tag{55}$$

The state variable T can be factored out of every term appearing in Eq. (20). Hence, by setting Eq. (20) to zero, $T_{TF} = 0$ is one of the roots. By setting $T = 0$, the population of Regulatory T cells (Regulatory T cells (Tregs)) cells, macrophages, T1-helper cells and natural killer cells in the tumor-free equilibrium points are derived as follows:

$$R_{TF}^* = \frac{wC^*}{u_R} \tag{56}$$

$$M_{1\,TF}^* = \frac{\varphi_1}{\Delta} \tag{57}$$

$$M_{2TF}^* = \frac{\varphi_3}{\Delta} \tag{58}$$

$$\Omega_{TF}^* = \lambda_{T_1M_1} T_0 \left(\frac{M_{1\,TF}^*}{M_{1\,TF}^* + K_{M_1}}\right)\left(\frac{\gamma_1 M_{1\,TF}^*}{\gamma_1 M_{1\,TF}^* + K_{I_{12}}}\right)\left(\frac{K_{I_{10}}}{K_{I_{10}} + \gamma_2 M_{2TF}^*}\right) \tag{59}$$

$$T_{1\,TF}^* = \frac{\Omega}{d_{T_1} - \lambda_{TI_2}\left(\frac{I_2}{I_2 + K_{I_2}}\right)} \tag{60}$$

$$N_{TF}^* = \frac{eC^*}{f + \frac{p_N I_2}{g_N + I_2}} \tag{61}$$

The population of CD8+ T cells is computed using the Eqs. (51) and (52) and setting $T = 0$:

$$L = \frac{\xi + I_2^*}{\omega I_2^*}\left(\mu_{I_2} I_2^* - \phi C^* - \lambda_{I_2T_1} T_1^*\right) \tag{62}$$

$$L\left(-\frac{\theta m}{\theta + I_2} + \frac{\beta_2 I_2}{k_2 + I_2} - \frac{uRI_2}{k_k + I_2} L\right) = 0 \tag{63}$$

Solving the Eqs. (62) and (63) gives the populations of CD8+ T cells and IL2. By substituting these two parameters in (56)-(61), other states in the tumor-free equilibrium point are derived.

ACCEPTED MANUSCRIPT

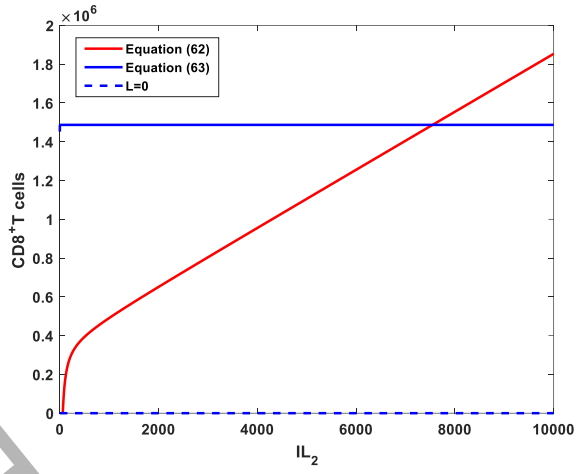


Fig. 7: The tumor-free equilibrium points. The intersections of Eqs. (62) and (63).

The tumor-free steady states are determined by solving Eqs. (62) and (63) together with the relationships given in Eqs. (56)–(61). Under the parameter values specified in Table 2, two distinct equilibria corresponding to the absence of tumor cells are identified, as depicted in Fig. 7. The numerical values of these equilibrium states are listed in Table 7. Based on the model presented in [39], only one tumor-free equilibrium point exists in the system, while based on Table 7, two tumor-free equilibrium states exist.

Table 7: Tumor-free steady states obtained for the parameter set specified in Table 2

	T_{TF}^*	N_{TF}^*	L_{TF}^*	C_{TF}^*	I_{2TF}^*	T_{1TF}^*	R_{TF}^*	M_{1TF}^*	M_{2TF}^*
E_{TF1}	0	3.33×10^{8}	0	3×10^{9}	60.91	4.95×10^{-4}	3.66×10^{7}	2.86×10^{3}	3.45×10^{2}
E_{TF2}	0	2.88×10^{8}	1.49×10^{6}	3×10^{9}	7.55×10^{3}	4.98×10^{-4}	3.66×10^{7}	2.86×10^{3}	3.45×10^{2}

the models presented in [38, 39], only two equilibrium states may exist. However, by the parameter set presented in Table 2, four states may occur for the patient. In two cases, there is no tumor cell in the body i.e. tumor-free equilibrium states, and in the other two cases, there are tumor cells in the body, and the treatment is essential i.e. tumor-present equilibrium states. The occurrence of each state depends on the initial state of the patient and the stability of these states.

3.3.2. Stability analysis:

Stability of the equilibrium is investigated through the indirect Lyapunov approach. Within this framework, the nonlinear system is linearized in the neighborhood of the equilibrium under consideration by evaluating its Jacobian matrix, after which the associated eigenvalues are determined. For the free system, the resulting Jacobian matrix is given by:

ACCEPTED MANUSCRIPT

$$J=\begin{bmatrix} f_{11} & f_{12} & f_{13} & 0 & 0 & f_{16} & f_{17} & f_{18} & 0 \\ f_{21} & f_{22} & 0 & f_{24} & f_{25} & 0 & 0 & 0 & 0 \\ f_{31} & f_{32} & f_{33} & f_{34} & f_{35} & 0 & f_{37} & 0 & 0 \\ 0 & 0 & 0 & f_{44} & 0 & 0 & 0 & 0 & 0 \\ 0 & 0 & f_{53} & f_{54} & f_{55} & f_{56} & 0 & 0 & 0 \\ 0 & 0 & 0 & 0 & f_{65} & f_{66} & 0 & f_{68} & f_{69} \\ f_{71} & 0 & 0 & f_{74} & f_{75} & 0 & f_{77} & 0 & 0 \\ f_{81} & 0 & 0 & 0 & 0 & 0 & 0 & f_{88} & f_{89} \\ f_{91} & 0 & 0 & 0 & 0 & 0 & 0 & f_{98} & f_{99} \end{bmatrix} \tag{64}$$

and,

$$f_{11}=a(1-bT)-baT-ce^{-\lambda_T R}N-\frac{(1-l)dsT^{l}L^{l}+dL^{2l}}{\left(sT^{l}+L^{l}\right)^{2}}-\delta_{m_1}M_1-\delta_{T_1}T_1$$

$$f_{12}=-ce^{-\lambda_T R}T$$

$$f_{13}=-\frac{sdlT^{l+1}L^{l-1}}{\left(sT^{l}+L^{l}\right)^{2}}$$

$$f_{16}=-\delta_{T_1}T$$

$$f_{17}=-\lambda_T ce^{-\lambda_T R}NT$$

$$f_{18}=-\delta_{m_1}T$$

$$f_{21}=-pN$$

$$f_{22}=-f-pT+\frac{p_N I_2}{g_N+I_2}$$

$$f_{24}=e$$

$$f_{25}=\frac{p_N g_N N}{\left(g_N+I_2\right)^{2}}$$

$$f_{31}=\frac{jkL}{\left(k+T\right)^{2}}-qL+r_1N+r_2C$$

$$f_{32}=r_1T$$

$$f_{33}=-\frac{\theta m}{\theta+I_2}-2\frac{uLRI_2}{k_k+I_2}+\frac{\beta_2 I_2}{k_2+I_2}+\frac{jT}{k+T}-qT$$

$$f_{34}=r_2T$$

$$f_{35}=\frac{\theta mL}{\left(\theta+I_2\right)^{2}}-\frac{uk_k L^2 R}{\left(k_k+I_2\right)^{2}}+\frac{k_2\beta_2 L}{\left(k_2+I_2\right)^{2}}$$

ACCEPTED MANUSCRIPT

$$f_{37} = -\frac{uL^2 I_2}{k_k + I_2}$$

$$f_{44} = -\beta$$

$$f_{53} = \frac{\omega I_2}{\xi + I_2}$$

$$f_{54} = \phi$$

$$f_{55} = -\mu_{I_2} + \frac{\omega \xi L}{\left(\xi + I_2\right)^2}$$

$$f_{56} = \lambda_{I_2 T_1}$$

$$f_{65} = \lambda_{TI_2} \frac{K_{I_2}}{(I_2 + K_{I_2})^2} T_1$$

$$f_{66} = -d_{T_1} + \lambda_{TI_2} \frac{I_2}{(I_2 + K_{I_2})}$$

$$f_{68} = \lambda_{T_1 M_1} T_0 \frac{K_{M_1}}{(M_1 + K_{M_1})^2} \left(\frac{\gamma_1 M_1}{\gamma_1 M_1 + K_{I_{12}}} \right) \left(\frac{K_{I_{10}}}{K_{I_{10}} + \gamma_2 M_2} \right) + \frac{\gamma_1 K_{I_{12}}}{\left(\gamma_1 M_1 + K_{I_{12}}\right)^2} \lambda_{T_1 M_1} T_0 \left(\frac{M_1}{M_1 + K_{M_1}} \right) \left(\frac{K_{I_{10}}}{K_{I_{10}} + \gamma_2 M_2} \right)$$

$$f_{69} = \frac{-\gamma_2 K_{I_{10}}}{\left(K_{I_{10}} + \gamma_2 M_2\right)^2} \lambda_{T_1 M_1} T_0 \left(\frac{M_1}{M_1 + K_{M_1}} \right) \left(\frac{\gamma_1 M_1}{\gamma_1 M_1 + K_{I_{12}}} \right)$$

$$f_{74} = w$$

$$f_{75} = \left(\frac{p_R R g_R}{\left(g_R + I_2\right)^2} \right) \left(\frac{\gamma_3 T}{\gamma_3 T + g_{T_\beta}} \right)$$

$$f_{77} = -u_R + \left(\frac{p_R I_2}{g_R + I_2} \right) \left(\frac{\gamma_3 T}{\gamma_3 T + g_{T_\beta}} \right)$$

$$f_{81} = -\left(\lambda_1 \gamma_3 + \lambda_2 \gamma_4\right) M_1$$

$$f_{88} = -K_1 - \left(\lambda_1 \gamma_3 + \lambda_2 \gamma_4\right) T$$

$$f_{89} = \nu$$

$$f_{91} = \left(\lambda_1 \gamma_3 + \lambda_2 \gamma_4\right) M_1$$

$$f_{98} = \left(\lambda_1 \gamma_3 + \lambda_2 \gamma_4\right) T$$

$$f_{99} = -K_2 - \nu$$

Table 8 reports the eigenvalue sets associated with the equilibrium states listed in Tables 6 and 7.

ACCEPTED MANUSCRIPT

Table 8: The eigenvalues of the equilibrium points presented in Tables 6 and 7

	λ_1	λ_2	λ_3	λ_4	λ_5	λ_6	λ_7	λ_8	λ_9
$E_{TF,1}$	–11.74	0.4309	0.0571	–0.058	–0.0385	–0.02	–0.197	–0.0125	–0.0063
$E_{TF,2}$	–8.841	–1.805	–0.8691	–0.058	–0.0385	–0.02	–0.196	–0.0105	–0.0063
$E_{TP,1}$	–858	–1.83	–3.57	0.4155	–0.0384	–0.0123	–0.008	–0.197	–0.0063
$E_{TP,2}$	–32845	–30.61	–6.055	–0.3802	–0.0213	–0.0121	–0.008	–0.1967	–0.0063

stability analysis confirms that both equilibrium states $E_{TF,2}$ corresponding to the tumor-free condition, and $E_{TF,2}$ representing the tumor-bearing state, are stable. In other words, in the absence of treatment, the eventual health status of the patient depends on the initial state of the system. A stronger immune response drives the system toward $\mathrm{E}_{\mathrm{TF},2}$ i.e. healthy state. Otherwise, the patient will be ill and the treatment is essential. Different initial states are considered in Table 9 for simulation.

4. Simulation results

This section presents a comprehensive analysis of the proposed tumor–immune interaction model. Section 4.1 investigates the existence and stability properties of the equilibrium points and identifies the conditions under which tumor elimination, tumor persistence, or coexistence may occur. Section 4.2 examines the local behavior of the system around the equilibrium states and provides further insight into the influence of model parameters on system stability. Finally, Section 4.3 presents numerical simulations and sensitivity analyses to illustrate the dynamic behavior of the model and to identify the biological mechanisms that most strongly influence tumor progression and immune response. Together, these analyses provide both theoretical and computational validation of the proposed framework and improve understanding of the underlying tumor–immune dynamics. Five different initial conditions are considered for the simulations (Table 9). In these scenarios, the initial populations of tumor cells, NK cells, CD8+ T cells, and circulating lymphocytes are changed, but the initial sizes of other states are kept fixed.

Table 9: The initial conditions used for simulation. The initial conditions for tumor cells, NK cells, and CD8+ T cells are varied and other initial conditions are kept fixed.

State	Initial values 1	Initial values 2	Initial values 3	Initial values 4	Initial values 5
Tumor cells	10^6	10^6	10^7	10^6	10^9
NK cells	10^3	10^5	10^5	10^5	10^3
CD8+ T cells	10	100	100	100	10
Circulating Lymphocytes	6×10^8	6×10^{10}	6×10^{10}	6×10^{10}	6×10^8
Interleukin 2	1073	1073	1073	1073	1073
T1 helper cells	0	0	0	0	0
Regulatory T cells (Tregs)	1	1	1	1	1
Macrophages M1	2000	2000	2000	2000	2000
Macrophages M2	2500	2500	2500	2500	2500

Moreover, three immune systems with different strengths are considered.

ACCEPTED MANUSCRIPT

The quantity D serves as an indicator of the overall potency of the immune response. Its magnitude is strongly dependent on the three parameters s, l and d each of which contributes substantially to the resulting immune-strength measure. Three cases are regarded, i.e. strong immune response, moderate immune response, and weak immune response (Table 10).

Table 10: Parameter settings associated with the three immune-response mechanisms

	s	l	d
Strong immune response	5×10^{-3}	1	2.1
Moderate immune response	8×10^{-3}	1.5	1.6
Weak immune response	4×10^{-2}	2	1.3

Although simulations were performed for all initial conditions listed in Table 9, only Cases 1 and 5 are shown in the figures because they represent the smallest and largest initial tumor burdens, respectively. The intermediate cases exhibited similar qualitative trends, differing primarily in the magnitude and timing of the responses. Therefore, Cases 1 and 5 were selected as representative scenarios to illustrate the full range of model behavior while preserving figure readability.

4.1. No treatment

The simulation results demonstrate the importance of the overall effectiveness of the immune response. For all initial states, a strong patient can overcome cancer in the absence of any treatment. The no-treatment behavior of the system with a strong immune response is shown in Fig. 8. The initial conditions 1 and 5 (Table 9) are regarded for simulation.

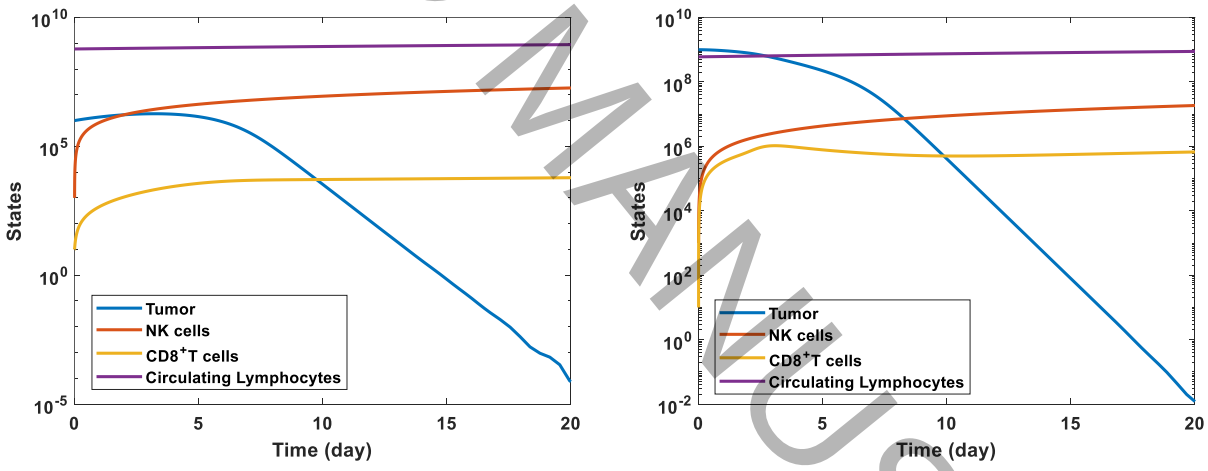
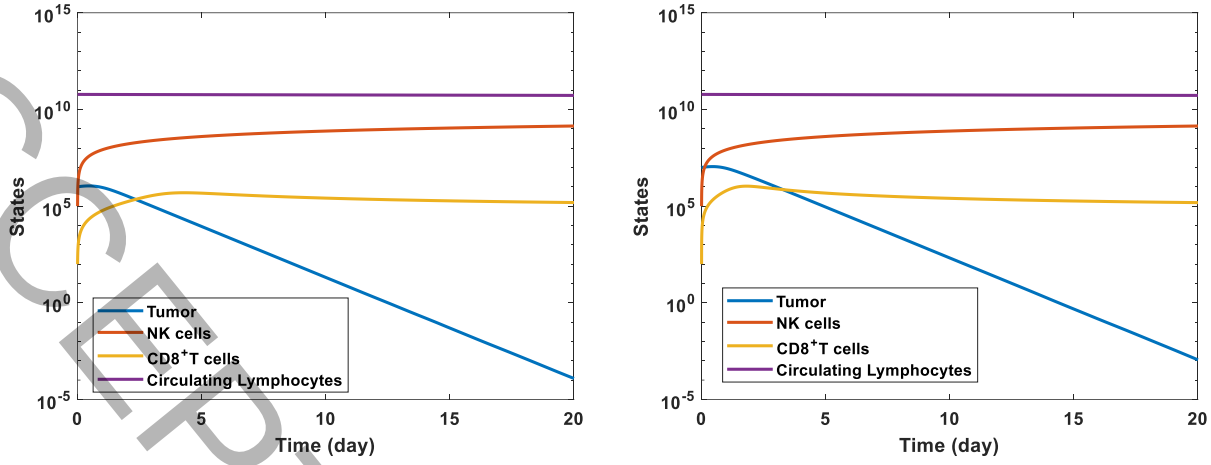


Fig. 8: The no-treatment behavior of a strong patient (Table 10). The initial conditions 1 and 5 (Table 9) are regarded for simulation. (a) Initial condition 1; (b) Initial condition 5.

A patient with a moderate immune response can overcome cancer only for some initial states, i.e. initial states 2 and 3. In other cases, cancer grows rapidly to its carrying capacity. The behavior of the system under a moderate immune response for initial states 2 and 3 are shown in Fig. 9.

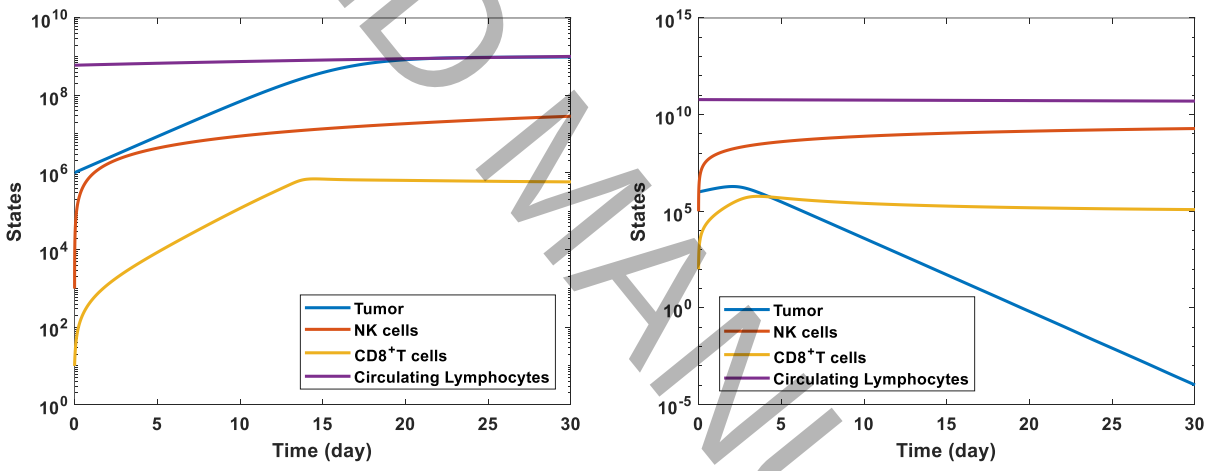
ACCEPTED MANUSCRIPT



(a) **(b)**

Fig. 9: The no-treatment behavior of a moderate patient (Table 10). The initial conditions 2 and 3 (Table 9) are regarded for simulation. (a) Initial condition 2; (b) Initial condition 3.

A weak patient can eliminate the tumor only under initial condition 2. The behavior of the weak patient with initial conditions 1 and 2 are shown in Fig. 10.



(a) **(b)**

Fig. 10: The no-treatment behavior of a weak patient (Table 10). The initial conditions 1 and 2 (Table 9) are regarded for simulation. (a) Initial condition 1; (b) Initial condition 2.

The number of days passed until the tumor population reaches 1 is presented in Table 10. In "fail" cases, the immune system cannot remove the tumor cells.

Table 11: The number of days in which the population of tumor cells reaches 1 in the absence of the treatment. In other cases, the immune system is unable to overcome cancer.

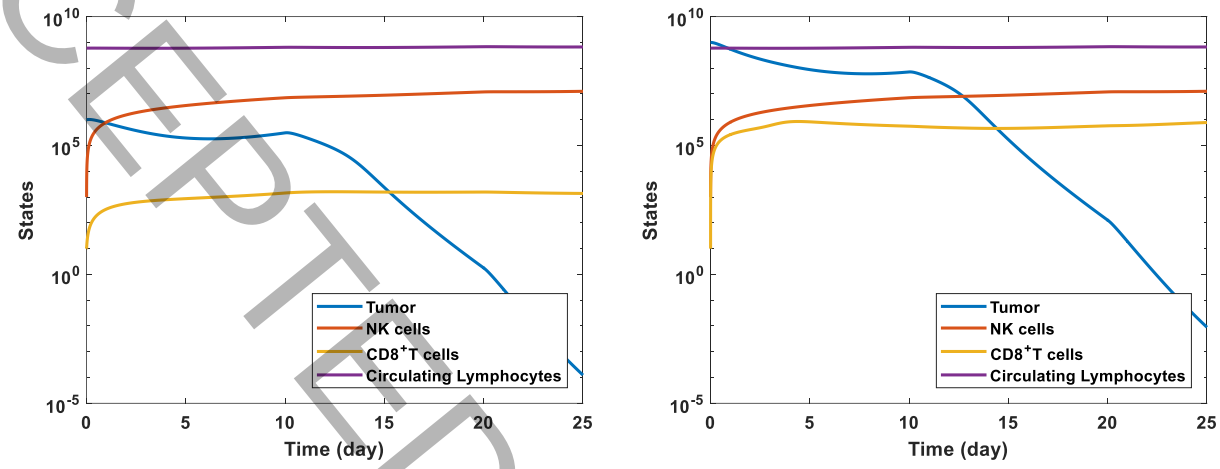
Initial condition	Weak	moderate	strong
1	Fail	Fail	14.78
2	18.46	12.5	8.37
3	Fail	14.38	9.72
4	Fail	Fail	11.12
5	Fail	Fail	17.52

ACCEPTED MANUSCRIPT

4.2. Chemotherapy

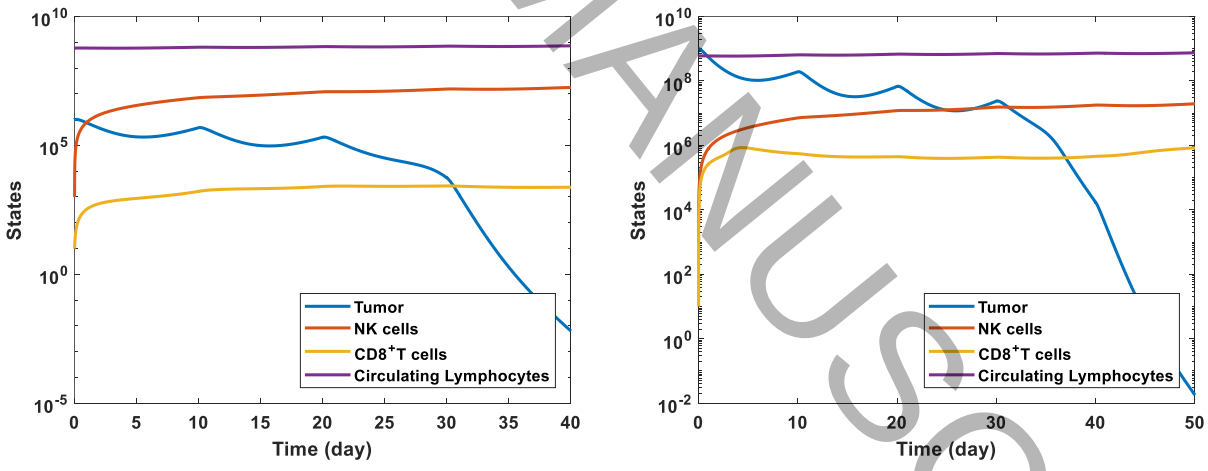
In this section, only chemotherapy treatment is applied. The chemo-dose is applied every 10 days with the dosage 2.3869 [39]. This dosage is recommended by the manufacturers of the drug Adria (doxorubicin HCI). This treatment strategy can remove cancer cells for all initial conditions regarded for the patient with a moderate immune response. The behavior of the system with moderate immune response with initial conditions 1 and 5 is shown in Fig. 11.

The proposed treatment can remove cancer cells for all initial conditions in the weak patient. The behavior of the system for initial conditions 1 and 5 are shown in Fig. 12.



(a) **(b)**

Fig. 11: The behavior of the system during chemotherapy in a patient with a moderate immune response (Table 10). The initial conditions 1 and 5 are regarded (Table 9). (a) Initial condition 1; (b) Initial condition 5.



(a) **(b)**

Fig. 12: The behavior of the system during chemotherapy in a weak patient (Table 10). The initial conditions 1 and 3 are regarded (Table 9). (a) Initial condition 1; (b) Initial condition 5.

The number of days passed during chemotherapy until the tumor population reaches 1 is presented in Table 11.

ACCEPTED MANUSCRIPT

Table 12: The number of days in which the population of tumor cells reaches 1 during chemotherapy.

Initial condition	weak	moderate
1	35.46	20.34
2	No need to treatment (Table 11)	No need to treatment(Table 11)
3	12.63	No need to treatment(Table 11)
4	32.37	11.66
5	46.29	22.43

4.3. Immunotherapy

Vaccines, immune response modifiers and monoclonal antibodies are three main categories of immunotherapy. Vaccines are therapeutic which are constructed from tumor cells. CSFs, TNFs, interferons, and interleukins such as IL-2 are immune response modifiers. Monoclonal antibodies can between normal and cancer cells. In this paper, immunotherapy consists of injecting IL-2 and CD8+ T cells. The dosage of IL2 is 2.7859×10^{6} and the dosage of CD8+ T cells is 1.77×10^{10}. They are injected every 10 days. The behavior of the system with a moderate immune response with initial conditions 1 and 5 is shown in Fig. 13.

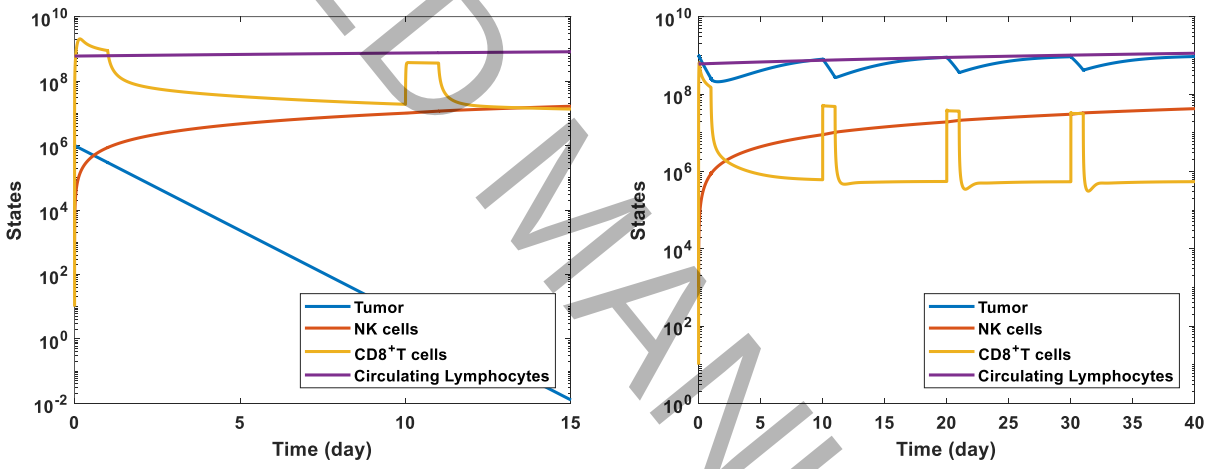


Fig. 13: the behavior of the system during chemotherapy in a patient with a moderate immune response (Table 10). The initial conditions 1 and 5 are regarded (Table 9). (a) Initial condition 1; (b) Initial condition 5.

ACCEPTED MANUSCRIPT

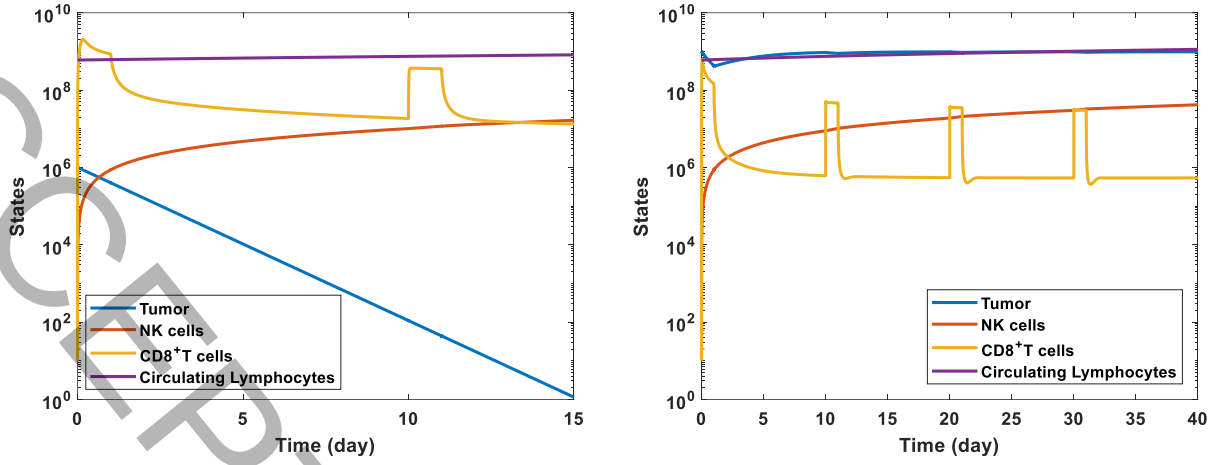


Fig. 14: the behavior of the system during chemotherapy in a weak patient (Table 10). The initial conditions 1 and 5 are regarded (Table 9). (a) Initial condition 1; (b) Initial condition 5.

The proposed treatment is able to remove cancer cells only in initial conditions 1 and 3 in the weak patient. In other initial conditions, the treatment strategy fails. Fig. 14 depicts the system dynamics corresponding to the two specified initial conditions, namely cases 1 and 5. The number of days passed during immunotherapy until the tumor population reaches 1 is presented in Table 12. If immunotherapy is started from day 10, the capability of immunotherapy is shown in Table 13. As shown in this table, immunotherapy cannot remove cancer cells in more cases. This shows the importance of the immune system strength and its population.

Table 12: The number of days in which the population of tumor cells reaches to 1 during immunotherapy.

Initial condition	weak	moderate
1	15.14	11.38
2	No need to treatment (Table 11)	No need to treatment(Table 11)
3	17.84	No need to treatment(Table 11)
4	Fail	15.68
5	Fail	Fail

Table 13: The number of days in which the population of tumor cells reaches to 1 during immunotherapy. Immunotherapy started from day 10.

Initial condition	weak	moderate
1	Fail	24.56
2	No need to treatment (Table 11)	No need to treatment(Table 11)
3	Fail	No need to treatment(Table 11)
4	Fail	Fail
5	Fail	Fail

ACCEPTED MANUSCRIPT

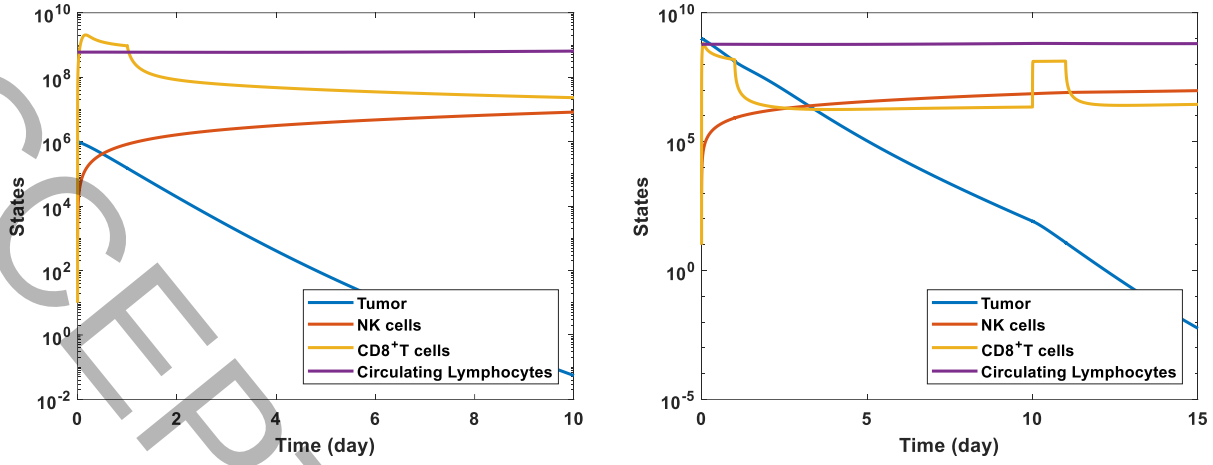


Fig. 15: The behavior of the system during chemo-immunotherapy in a patient with a moderate immune response (Table 10). The initial conditions 1 and 5 are regarded (Table 9). (a) Initial condition 1; (b) Initial condition 5.

4.4. Chemo-immunotherapy

This treatment strategy is able to remove cancer in all initial conditions. The behavior of the system with a moderate immune response with initial conditions 1 and 5 are shown in Fig. 15. The behavior of the system with a weak immune response during chemo-immunotherapy with initial conditions 1 and 5 are shown in Fig. 16.

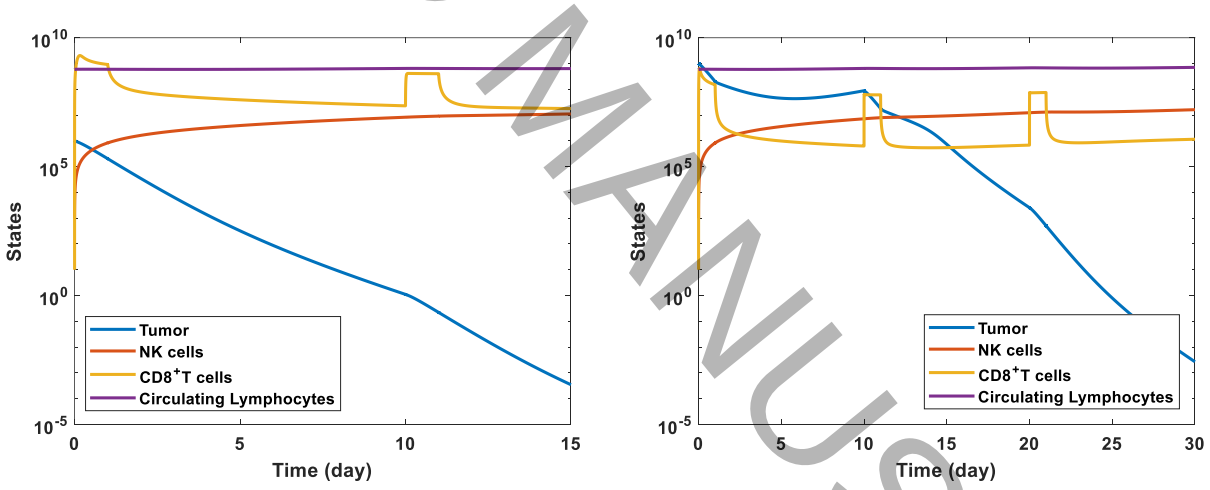


Fig. 16: The behavior of the system during chemo-immunotherapy in a weak patient (Table 10). The initial conditions 1 and 5 are regarded (Table 9). (a) Initial condition 1; (b) Initial condition 5.

The number of days passed during chemo-immunotherapy until the tumor population reaches 1 is presented in Table 14.

ACCEPTED MANUSCRIPT

Table 14: The number of days in which the population of tumor cells reaches to 1 during chemo-immunotherapy.

Initial condition	weak	moderate
1	10.09	7.83
2	No need to treatment (Table 11)	No need to treatment(Table 11)
3	11.45	No need to treatment(Table 11)
4	13.58	10.92
5	24.83	12.21

5. Discussion

The proposed model extends the tumor–immune framework of De Pillis et al. by incorporating macrophage polarization, cytokine-mediated feedback loops, and immune-strength dynamics. The analysis demonstrated that the model preserves biologically meaningful behavior since all state variables remain non-negative and the system possesses both tumor-free and tumor-present equilibrium points. Furthermore, the existence of stable tumor-free and tumor-present equilibria indicates that tumor progression depends not only on treatment but also on the initial immune status and tumor burden.

The sensitivity analysis revealed that, besides the tumor proliferation rate and carrying capacity, parameters associated with immune-system strength have a major influence on tumor dynamics. In particular, the parameter lll, which directly affects immune-mediated tumor killing, was identified as one of the dominant parameters governing tumor progression. This observation is consistent with previous studies showing that immune competence is a critical determinant of treatment success.

The treatment simulations further highlighted the importance of immune-system strength. For patients with strong immune responses, all investigated initial conditions converged to tumor elimination without treatment. In contrast, patients with moderate and weak immune responses often required therapeutic intervention. These findings suggest that immune competence may significantly influence treatment selection and outcome.

Comparison of treatment strategies showed that chemotherapy alone successfully eliminated tumors in all considered cases, although the required treatment duration increased substantially for larger tumor burdens. For example, under weak immune response conditions, the elimination time ranged from 12.63 to 46.29 days depending on the initial condition. Immunotherapy alone was less robust, failing in several scenarios, particularly for larger tumors and weaker immune responses. In contrast, chemo-immunotherapy achieved tumor elimination in all investigated cases and generally reduced the required treatment time. For instance, in the largest tumor scenario (initial condition 5), the elimination time decreased from 46.29 days with chemotherapy alone to 24.83 days using chemo-immunotherapy under weak immune response conditions.

These findings are consistent with clinical and theoretical studies reporting improved outcomes for combined chemo-immunotherapy compared with monotherapies. The results also support recent evidence that effective cancer treatment should simultaneously target tumor-cell proliferation and reinforce anti-tumor immune activity.

Despite these promising results, the model remains a simplified representation of tumor–immune interactions. Spatial heterogeneity, angiogenesis, tumor vasculature, pharmacokinetic variability, and detailed tumor microenvironment dynamics are not explicitly included. Future work will focus on incorporating these mechanisms and extending the framework toward patient-specific treatment optimization.

The obtained results are consistent with clinical tests [52-54]. Clinical advances in chemo-immunotherapy were presented in [52]. In [53], the successfulness of chemo-immunotherapy in patients with advanced NSCLC has been considered. It is shown that chemo-immunotherapy is more effective than chemotherapy alone. New trends in chemo-immunotherapy have been studied in [54]. However, the authors have stated that optimal dosing, timing, etc. are an open problem.

ACCEPTED MANUSCRIPT

Specifically, both the present model and the De Pillis framework ([35-39]) predict several common qualitative behaviors:

- Tumor elimination under sufficiently strong immune responses: In both models, enhancement of anti-tumor immune activity can drive tumor populations toward extinction.
- Tumor persistence under immune suppression: Both models predict that weakened immune activity or increased immunosuppressive influences lead to sustained tumor growth.
- Existence of multiple dynamical outcomes: Depending on parameter values and initial conditions, both models exhibit qualitatively different regimes including tumor elimination, tumor dormancy, and tumor escape.
- Sensitivity to immune-cell effectiveness: In both studies, the outcome is highly sensitive to the efficacy of immune effector populations, particularly cytotoxic T lymphocytes.

Furthermore, the present model extends the De Pillis framework by explicitly incorporating macrophage polarization (M1/M2), regulatory immune-cell populations, and cytokine-mediated feedback loops. Despite these additional mechanisms, the model reproduces the same fundamental tumor–immune competition dynamics reported in De Pillis et al. [35-39], which supports the biological plausibility of the proposed formulation.

The results of this study have both theoretical and practical implications for chemo-immunotherapy modeling. From a theoretical perspective, the proposed model demonstrates that tumor progression is governed by a complex interplay between intrinsic tumor-growth mechanisms and immune-regulatory processes. The sensitivity analysis revealed that parameters associated with immune competence exert an influence comparable to that of classical tumor-growth parameters, indicating that treatment outcomes depend not only on tumor aggressiveness but also on the effectiveness of the host immune response. This observation supports the growing recognition that immune-system status is a critical determinant of cancer progression and therapeutic success.

From a biological perspective, the model highlights the importance of macrophage polarization and cytokine-mediated feedback mechanisms in shaping the tumor microenvironment. The results suggest that promoting M1-associated anti-tumor responses while suppressing M2-associated immunosuppressive pathways may significantly improve tumor control. These findings are consistent with recent experimental and clinical studies investigating macrophage repolarization and immune-modulating therapies as complementary approaches to conventional cancer treatment.

The present work also contributes to the broader field of tumor–immune mathematical modeling. Classical models, such as those developed by [35] and later by [36-39], established the fundamental role of immune effector cells in tumor control. The proposed framework extends these approaches by incorporating additional regulatory components, including macrophage phenotypic plasticity, immune-strength dynamics, and cytokine-driven feedback loops. Consequently, the model provides a more comprehensive description of the regulatory mechanisms that influence treatment outcomes.

Although the current study is not intended to provide patient-specific predictions, the results demonstrate how mathematical models can be used to identify influential biological pathways, prioritize therapeutic targets, and evaluate the relative importance of different immune mechanisms. These capabilities may ultimately support the design and optimization of combined chemo-immunotherapy strategies and contribute to the development of more personalized cancer treatment approaches.

Despite the insights provided by the proposed model, several limitations should be acknowledged. First, the model adopts a non-spatial ordinary differential equation framework and therefore does not explicitly represent the heterogeneous tumor microenvironment. Important biological processes such as extracellular matrix remodeling, hypoxia, nutrient gradients, mechanical stresses, cell migration, and spatial variations in immune-cell infiltration are not included. Recent studies have shown that these factors can significantly influence macrophage polarization, immune suppression, tumor progression, and treatment efficacy. Consequently, the present model should be interpreted as a population-level representation of tumor–immune interactions rather than a detailed description of local tumor microenvironment dynamics.

A second limitation is the absence of explicit tumor vasculature and angiogenesis. The formation of vascular networks plays a critical role in supplying oxygen and nutrients to tumor tissues, facilitating immune-cell trafficking, and regulating drug delivery. Since vascular-mediated transport mechanisms are not represented in the current framework,

ACCEPTED MANUSCRIPT

the model cannot capture phenomena associated with abnormal vascularization, hypoxic regions, or vascular normalization therapies.

In addition, treatment administration is modeled using simplified effective therapeutic terms. Although this approach enables the investigation of chemotherapy, immunotherapy, and combined chemo-immunotherapy within a tractable mathematical framework, it does not account for detailed pharmacokinetic and pharmacodynamic processes, drug metabolism, toxicity accumulation, treatment scheduling, resistance development, or patient-specific dosing protocols. Therefore, the model is more suitable for studying qualitative treatment trends and mechanistic interactions than for optimizing clinical treatment regimens.

Finally, the model does not account for tumor heterogeneity, clonal evolution, genetic mutations, or stochastic fluctuations in cellular populations. Future work will focus on extending the framework by incorporating spatial tumor microenvironment dynamics, angiogenesis, vascular-mediated transport, macrophage migration, detailed treatment protocols, and patient-specific parameter identification. Such developments would improve biological realism and further enhance the applicability of mathematical modeling to personalized chemo-immunotherapy design.

6. Conclusion

A mathematical model of tumor–immune interactions under chemo-immunotherapy was developed by incorporating macrophage polarization, cytokine dynamics, and immune-strength regulation. The model was shown to possess non-negative solutions and four equilibrium points, including stable tumor-free and tumor-present states. Sensitivity analysis demonstrated that, in addition to tumor proliferation rate and carrying capacity, immune-strength-related parameters are among the most influential factors affecting tumor growth. Numerical simulations showed that:

- A strong immune system eliminated tumors without treatment for all five investigated initial conditions.
- Immunotherapy alone failed in several weak- and moderate-immunity scenarios.
- Chemotherapy alone successfully removed tumors but often required long treatment durations, reaching 46.29 days in the most challenging scenario.
- Chemo-immunotherapy eliminated tumors in all investigated cases and reduced treatment duration to as little as 7.83 days for moderate immune response and 24.83 days for the most challenging weak-immunity scenario.

Overall, the results demonstrate that immune-system strength is a key determinant of treatment outcome and that chemo-immunotherapy provides the most robust strategy across a wide range of tumor burdens and immune conditions.

ACCEPTED MANUSCRIPT

Ethical approval: No ethics approval was required
Conflict of interest: The authors declare that they have no conflicts of interest.
Funding: No funding was received for this study.
Data availability: Not applicable
Clinical trial number: not applicable.
Ethics and Consent to Participate declarations: not applicable.
Consent to Publish declaration: not applicable.

ACCEPTED MANUSCRIPT

7. References

[1] R.L. Siegel, T.B. Kratzer, N.S. Wagle, H. Sung, A. Jemal, Cancer statistics, 2026, CA: A Cancer Journal for Clinicians, 76(1) (2026).

[2] H.C. Wei, J.T. Lin, Periodically pulsed immunotherapy in a mathematical model of tumor-immune interaction, International Journal of Bifurcation and Chaos, 23(4) (2013).

[3] E.W. Curren Smith, Macrophage Polarization and Its Role in Cancer, Journal of Clinical & Cellular Immunology, 06(04) (2015).

[4] G.E. Mahlbacher, K.C. Reihmer, H.B. Frieboes, Mathematical modeling of tumor-immune cell interactions, Journal of Theoretical Biology, 469 (2019) 47–60.

[5] H. Zhang, C. Li, Mathematical modelling of tumor-immune interactions in breast cancer, Journal of Theoretical Biology, 618 (2026).

[6] R.D. Leek, C.E. Lewis, R. Whitehouse, M. Greenall, J. Clarke, A.L. Harris, Association of macrophage infiltration with angiogenesis and prognosis in invasive breast carcinoma, Cancer Research, 56(20) (1996) 4625–4629.

[7] K.A.O. Ellem, M.G.E. O'Rourke, G.R. Johnson, G. Parry, I.S. Misko, C.W. Schmidt, P.G. Parsons, S.R. Burrows, S. Cross, A. Fell, C.L. Li, J.R. Bell, P.J. Dubois, D.J. Moss, M.F. Good, A. Kelso, L.K. Cohen, G. Dranoff, R.C. Mulligan, A case report: Immune responses and clinical course of the first human use of granulocyte/macrophage-colony-stimulating-factor-transduced autologous melanoma cells for immunotherapy, Cancer Immunology Immunotherapy, 44(1) (1997) 10–20.

[8] J. Mattes, M. Hulett, W. Xie, S. Hogan, M.E. Rothenberg, P. Foster, C. Parish, Immunotherapy of cytotoxic T cell-resistant tumors by T helper 2 cells: An eotaxin and STAT6-dependent process, Journal of Experimental Medicine, 197(3) (2003) 387–393.

[9] S.M. Hsu, J.W. Waldron, P.L. Hsu, A.J. Hough, Cytokines in malignant lymphomas: Review and prospective evaluation, Human Pathology, 24(10) (1993) 1040–1057.

[10] L. Bingle, N.J. Brown, C.E. Lewis, The role of tumour-associated macrophages in tumour progression: Implications for new anticancer therapies, Journal of Pathology, 196(3) (2002) 254–265.

[11] L.S. Hammes, R.R. Tekmal, P. Naud, M.I. Edelweiss, N. Kirma, P.T. Valente, K.J. Syrjänen, J.S. Cunha-Filho, Macrophages, inflammation and risk of cervical intraepithelial neoplasia (CIN) progression-Clinicopathological correlation, Gynecologic Oncology, 105(1) (2007) 157–165.

[12] I. Lampropoulos, P.G. Kevrekidis, C.E. Zois, H. Byrne, M. Kavousanakis, Spatio-Temporal Dynamics of M1 and M2 Macrophages in a Multiphase Model of Tumor Growth, Bulletin of Mathematical Biology, 87(7) (2025).

[13] J.J. Bosque, J. Martínez, J.G. Otero, G. Aguadé-Gorgorió, J.E. Sanchez-Galan, J. Belmonte-Beitia, Mathematical model of tumor-macrophage dynamics in glioma to advance myeloid-targeted therapies, Computers in Biology and Medicine, 196 (2025).

[14] A.C. la Flamme, M. Kharkrang, S. Stone, S. Mirmoeini, D. Chuluundorj, R. Kyle, Type II-Activated Murine Macrophages Produce IL-4, PLoS ONE, 7(10) (2012).

[15] M.F. Neurath, S. Fichtner-Feigl, R. Kesselring, Intestinal Inflammation and Cancer of the Gastrointestinal Tract, Mucosal Immunology: Fourth Edition, 2-2 (2015) 1761–1775.

[16] W.J. Chen, W. Jin, N. Hardegen, K.J. Lei, L. Li, N. Marinos, G. McGrady, S.M. Wahl, Conversion of Peripheral CD4+CD25- Naive T Cells to CD4+CD25+ Regulatory T Cells by TGF-β Induction of Transcription Factor Foxp3, Journal of Experimental Medicine, 198(12) (2003) 1875–1886.

[17] A.Y. Mitrophanov, E.A. Groisman, Positive feedback in cellular control systems, BioEssays, 30(6) (2008) 542–555.

[18] N.T. Ingolia, A.W. Murray, Positive-Feedback Loops as a Flexible Biological Module, Current Biology, 17(8) (2007) 668–677.

[19] V. Morales, L. Soto-Ortiz, Modeling Macrophage Polarization and Its Effect on Cancer Treatment Success, Open Journal of Immunology, 08(02) (2018) 36–80.

[20] H. Zhang, Y. Qu, W. Yang, C. Li, Mathematical model of tumor-macrophage interactions: Elucidating the tumor-driven macrophage phenotype reprogramming, Journal of Theoretical Biology, 629 (2026).

[21] E. Bastiaannet, J.C. Beukema, H.J. Hoekstra, Radiation therapy following lymph node dissection in melanoma patients: Treatment, outcome and complications, Cancer Treatment Reviews, 31(1) (2005) 18–26.

[22] D. Shakir, Chemotherapy Induced Cardiomyopathy: Pathogenesis, Monitoring and Management, Journal of Clinical Medicine Research, (2009).

[23] S.A. Rosenberg, N.P. Restifo, Adoptive cell transfer as personalized immunotherapy for human cancer, Science, 348(6230) (2015) 62–68.

ACCEPTED MANUSCRIPT

[24] S. Van Lint, S. Wilgenhof, C. Heirman, J. Corthals, K. Breckpot, A. Bonehill, B. Neyns, K. Thielemans, Optimized dendritic cell-based immunotherapy for melanoma: The TriMix-formula, Cancer Immunology, Immunotherapy, 63(9) (2014) 959–967.
[25] D.S. Rodrigues, P.F.A. Mancera, T. Carvalho, L.F. Gonçalves, A mathematical model for chemoimmunotherapy of chronic lymphocytic leukemia, Applied Mathematics and Computation, 349 (2019) 118–133.
[26] A. Kumar, M. Bhargava, U.S. Dubey, B. Dubey, Impact of chemo-immunotherapy on tumour-immune interactions: A non-autonomous Model of Tumour Necrosis Factor and T cell dynamics, Computers in Biology and Medicine, 197 (2025).
[27] D. Hanahan, R.A. Weinberg, Hallmarks of cancer: The next generation, Cell, 144(5) (2011) 646–674.
[28] M. Nazari, A. Ghaffari, The effect of finite duration inputs on the dynamics of a system: Proposing a new approach for cancer treatment, International Journal of Biomathematics, 8(3) (2015).
[29] D.S. Rodrigues, P.F.A. Mancera, T. Carvalho, L.F. Gonçalves, Sliding mode control in a mathematical model to chemoimmunotherapy: The occurrence of typical singularities, Applied Mathematics and Computation, 387 (2020).
[30] M. Nazari, N. Babaei, Hybrid Nonlinear Adaptive Fuzzy Control Approach for Individualized Mixed Vaccine and Chemotherapy, Iranian Journal of Science and Technology, Transactions of Electrical Engineering, (2026).
[31] V.A. Kuznetsov, I.A. Makalkin, M.A. Taylor, A.S. Perelson, Nonlinear dynamics of immunogenic tumors: Parameter estimation and global bifurcation analysis, Bulletin of Mathematical Biology, 56(2) (1994) 295–321.
[32] D. Kirschner, J.C. Panetta, Modeling immunotherapy of the tumor - Immune interaction, Journal of Mathematical Biology, 37(3) (1998) 235–252.
[33] Y. Dong, R. Miyazaki, Y. Takeuchi, Mathematical modeling on helper t cells in a tumor immune system, Discrete and Continuous Dynamical Systems - Series B, 19(1) (2014) 55–72.
[34] H. Moore, N.K. Li, A mathematical model for chronic myelogenous leukemia (CML) and T cell interaction, Journal of Theoretical Biology, 227(4) (2004) 513–523.
[35] L.G. De Pillis, A. Radunskaya, A mathematical tumor model with immune resistance and drug therapy: An optimal control approach, Journal of Theoretical Medicine, 3(2) (2001) 79–100.
[36] L.G. De Pillis, A. Radunskaya, The dynamics of an optimally controlled tumor model: A case study, Mathematical and Computer Modelling, 37(11) (2003) 1221–1244.
[37] L.G. De Pillis, A.E. Radunskaya, C.L. Wiseman, A validated mathematical model of cell-mediated immune response to tumor growth, Cancer Research, 65(17) (2005) 7950–7958.
[38] L.G. De Pillis, W. Gu, A.E. Radunskaya, Mixed immunotherapy and chemotherapy of tumors: Modeling, applications and biological interpretations, Journal of Theoretical Biology, 238(4) (2006) 841–862.
[39] L. de Pillis, K.R. Fister, W. Gu, C. Collins, M. Daub, D. Gross, J. Moore, B. Preskill, Mathematical model creation for cancer chemo-immunotherapy, Computational and Mathematical Methods in Medicine, 10(3) (2009) 165–184.
[40] C.S. Tam, M.J. Keating, Chemoimmunotherapy of chronic lymphocytic leukemia, Best Practice and Research: Clinical Haematology, 20(3) (2007) 479–498.
[41] S. Sharma, G.P. Samanta, Analysis of the Dynamics of a Tumor–Immune System with Chemotherapy and Immunotherapy and Quadratic Optimal Control, Differential Equations and Dynamical Systems, 24(2) (2016) 149–171.
[42] N. Darandis, M. Nazari, A NEW MATHEMATICAL MODELING and SUB-OPTIMAL CHEMOTHERAPY of CANCER, Journal of Biological Systems, 29(3) (2021) 647–685.
[43] Y. Louzoun, C. Xue, G.B. Lesinski, A. Friedman, A mathematical model for pancreatic cancer growth and treatments, Journal of Theoretical Biology, 351 (2014) 74–82.
[44] N.Y. den Breems, R. Eftimie, The re-polarisation of M2 and M1 macrophages and its role on cancer outcomes, Journal of Theoretical Biology, 390 (2016) 23–39.
[45] A. Diefenbach, E.R. Jensen, A.M. Jamieson, D.H. Raulet, Rae1 and H60 ligands of the NKG2D receptor stimulate tumour immunity, Nature, 413(6852) (2001) 165–171.
[46] K.J. Mahasa, R. Ouifki, A. Eladdadi, L.d. Pillis, Mathematical model of tumor–immune surveillance, Journal of Theoretical Biology, 404 (2016) 312–330.
[47] S.R. Nielsen, M.C. Schmid, Macrophages as Key Drivers of Cancer Progression and Metastasis, Mediators of Inflammation, 2017 (2017).
[48] T. Chanmee, P. Ontong, K. Konno, N. Itano, Tumor-associated macrophages as major players in the tumor microenvironment, Cancers, 6(3) (2014) 1670–1690.
[49] R. Aogo, F. Nyabadza, Modelling the dynamics of HIV-related non-Hodgkin lymphomas in the presence of HIV treatment and chemotherapy, Mathematical Methods in the Applied Sciences, 41(18) (2018) 8385–8406.

ACCEPTED MANUSCRIPT

[50] P. Chen, Y. Huang, R. Bong, Y. Ding, N. Song, X. Wang, X. Song, Y. Luo, Tumor-associated macrophages promote angiogenesis and melanoma growth via adrenomedullin in a paracrine and autocrine manner, Clinical Cancer Research, 17(23) (2011) 7230–7239.
[51] M. Robertson-Tessi, A. El-Kareh, A. Goriely, A model for effects of adaptive immunity on tumor response to chemotherapy and chemoimmunotherapy, Journal of Theoretical Biology, 380 (2015) 569–584.
[52] D.R. Principe, S.D. Kamath, M. Korc, H.G. Munshi, The immune modifying effects of chemotherapy and advances in chemo-immunotherapy, Pharmacology and Therapeutics, 236 (2022).
[53] J. Jiao, W.W. Li, Y.H. Shang, X.F. Li, M. Jiao, Clinical effects of Chemotherapy combined with Immunotherapy in patients with advanced NSCLC and the effect on their nutritional status and immune function, Pakistan Journal of Medical Sciences, 39(2) (2023) 404–408.
[54] C. Sordo-Bahamonde, S. Lorenzo-Herrero, A.P. Gonzalez-Rodriguez, A. Martínez-Pérez, J.P. Rodrigo, J.M. García-Pedrero, S. Gonzalez, Chemo-Immunotherapy: A New Trend in Cancer Treatment, Cancers, 15(11) (2023).

ACCEPTED MANUSCRIPT